Nanomechanical behavior of yttria stabilized zirconia (YSZ) based thermal barrier coating

Nath, S., Mann, I., Majumbdar, JD

DOI 10.1016/j.ceramint.2014.11.039
ISSN 0272-8842
ESSN 1873-3956

Publisher: Science Direct

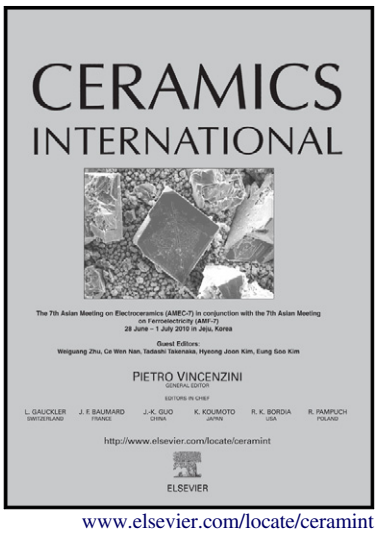

www.elsevier.com/locate/ceramint

Nanomechanical behavior of yttria stabilized zirconia (YSZ) based thermal barrier coating

Subhasisa Nath, Indranil Manna, Jyotsna Dutta Majumdar

PII: S0272-8842(14)01777-5
DOI: http://dx.doi.org/10.1016/j.ceramint.2014.11.039
Reference: CERI9484

To appear in: *Ceramics International*

Received date: 21 August 2014
Revised date: 5 November 2014
Accepted date: 5 November 2014

Cite this article as: Subhasisa Nath, Indranil Manna, Jyotsna Dutta Majumdar, Nanomechanical behavior of yttria stabilized zirconia (YSZ) based thermal barrier coating, *Ceramics International,* http://dx.doi.org/10.1016/j.ceramint.2014.11.039

Nanomechanical Behavior of Yttria Stabilized Zirconia (YSZ) based Thermal Barrier Coating

Subhasisa Nath[a1], Indranil Manna[a,b2], Jyotsna Dutta Majumdar[a, 3*]

[a]Department of Metallurgical and Materials Engineering, Indian Institute of Technology, Kharagpur 721302, West Bengal, India
[b]Indian Institute of Technology, Kanpur 208016, Uttar Pradesh, India
[1]:sendsubha@gmail.com; [2]:imanna@metal.iitkgp.ernet.in; [3]:jyotsna@metal.iitkgp.ernet.in

Abstract

In the present study, the detailed evaluation of nanomechanical properties in terms of hardness and Young's modulus of duplex and compositionally graded YSZ based thermal barrier coating (TBC) have been evaluated by nanoindentation technique. Duplex and compositionally graded TBCs have been fabricated by thermal spray deposition technique. As TBCs are commonly applied for high temperature protection, effect of isothermal treatment in air (at 900 °C and 1000 °C) on nanomechanical properties has also been evaluated. Finally, the mechanical properties have been correlated with characteristics of the coating. The hardness and Young's modulus of the TBCs are found to increase with increased duration of thermal exposure. Modulus of resilience and resistance to plastic deformation of the duplex and compositionally graded TBC have also been evaluated at room temperature and with thermal exposure and discussed in details.

Keywords: B. Porosity; C. Mechanical properties; Thermal barrier coating; Nanoindentation
*Corresponding author, FAX: +91-3222-282280

1. Introduction

Thermal barrier coating usually consists of low thermal conductivity ceramics usually composed of 7- 8 wt% yttria stabilized zirconia (YSZ) deposited by plasma spraying onto the surface of bond coated (MCrAlY, where M= Co, Ni or both) superalloy substrates to protect it from high temperature degradation [1-3]. . The failure of of TBC system is caused by the stress generated because of (a) thermal expansion mismatch between the ceramic top coat and metallic bond coat or substrate and (b) growth of thermally grown oxide (TGO) layer formed on the surface of bond coat during service [4, 5]. The level of stress in the conventional TBC may be minimized by application of a functionally graded coating [6-9]. In the past, it was also reported that the compositionally graded thermal barrier coating fabricated by plasma spray deposition offered an improved oxidation resistance as compared to duplex coating by forming protective Al_2O_3 scales in the graded layers, whose growth rate is slower that the same formed in conventional TBC [10-12]. The change in mechanical properties of the ceramic coating in service affects the life time of the component [13]. In the past, several studies were conducted to evaluate the variation of mechanical properties of zirconia based thermal barrier coatings with isothermal aging at temperature ranging from 1000 °C to 1400 °C for 2 h to 200 h [14–20]. Furthermore, it was also concluded that the mechanical properties (hardness and Young's modulus) of thermal barrier coating developed by plasma spray deposition technique were dependent on the microstructure of the TBC [21, 22]. A large variation in mechanical properties is usually noticed in the coated region due to formation of inhomogeneous microstructure [15, 23, 24, 25]. The hardness and Young's modulus values of EBPVD coated YSZ measured by

nanoindentation technique are found to vary from 3 GPa to 9 GPa and 80 GPa to 200 GPa , respectively [26]. It is also reported that the Young's modulus of the ceramic top coat increases with increase in annealing time from 2 h to 200 h and temperature from 1100 °C to 1300 °C [18, 19, 23]. Alfano *et al.* [17] measured the hardness and Young's modulus of plasma sprayed CeO_2-Y_2O_3-ZrO_2 based TBC with annealing time ranging from 2 h to 50 h at a constant temperature of 1315 °C. It is also concluded that improvement in mechanical properties with thermal exposure is attributed to decrease in porosity content in the coating due to sintering [17, 27]. The mechanical properties of the TBC due to hot corrosion are also reported by Afrasiabi *et al.* [16].

In the present study, hardness and Young's modulus of duplex and graded yttria stabilized zirconia (YSZ) based thermal barrier coatings are evaluated by nanoindentation technique in as-sprayed conditions and after thermal aging , and then correlated with their microstructure.

2. Experimental

Ni-based superalloys (Inconel 718) have been used as substrates for the development of duplex and compositionally graded TBCs by thermal spraying. Commercially available CoNiCrAlY alloy powder (Co-32Ni-21Cr-8Al-0.5Y in wt.%: MEC 9950AM) with particle size varying between 15 μm to 45 μm and 7 wt% Y_2O_3 stabilized ZrO_2 (7YSZ) powder (Amperit 831.007) with particle size ranging between 15 μm to 85 μm have been used as the precursor powders for the fabrication of TBC. Figs. 1 (a, b) show the scanning electron micrographs of (a) YSZ and (b) CoNiCrAlY used as feedstock powders for coating. From

Figure 1 it may be noted that the morphology of both the feedstock powders is spherical in shape. The spherical shape of powder particles ensures better flowability during spraying operation. Figs. 2 (a, b) show the x-ray diffraction profiles of (a) YSZ and (b) CoNiCrAlY feedstock powders used for coating development. From Fig. 2a, it is evident that the YSZ powder contains single phase tetragonal zirconia (t –ZrO_2) phase. Fig. 2b shows the presence of γ' -Ni_3Al and β –CoAl phases in γ –Co matrix. The β –CoAl phase acts as an aluminum reservoir which helps in the formation of Al_2O_3 scales during high temperature aging of TBC. The bond coat has been developed on sand blasted Inconel 718 substrate by HVOF spraying technique. Followed by the development of bond coat, the top coat (8YSZ) is developed by plasma spray deposition. The details of the development of duplex TBC and compositionally graded TBC have been discussed elsewhere [12]. Followed by coating, the coated components are subjected to isothermal aging at 900 °C and 1000 °C in air. The characteristics of the thermal barrier coating in as-sprayed condition and after isothermal aging are analyzed in terms of microstructure, phase and residual stress. The mechanical properties of the as-sprayed and the heat treated thermal barrier coatings are evaluated in terms of hardness, *H* and elastic modulus, *E*, by nanoindentation technique on both the top surface and along the cross-section. Nanoindentation tests are carried out using a nanoindenter (Hysitron-TI950 Triboindentor) with a Berkovich tip (tip radius < 150 nm) at a maximum load of 8 mN. Hardness is calculated by using the following equation:

$$H = \frac{P_{\max}}{A_C} \qquad (1)$$

where, P_{max} is the maximum load applied to the indenter and A_C is the projected area between the indenter and the specimen which is given by:

$$A_C \approx 24.5h_C^2 \quad (2)$$

Where, h_C is the contact depth expressed as [28]:

$$h_C = h_{max} - \varepsilon \frac{P_{max}}{S} \quad (3)$$

where, ε is the geometric constant with a value of 0.72 [28]. S is the stiffness measured by slope of the unloading curve and is given by:

$$S = \frac{dP}{dh} \quad (4)$$

The reduced modulus, E_r, obtained from the slope of initial portion of unloading curve, is given by the following equation [29]:

$$E_r = \frac{1}{2\beta h_C}\sqrt{\frac{\pi}{24.5}}\left(\frac{dP}{dh}\right) \quad (5)$$

$$\frac{1}{E_r} = \frac{1-\upsilon^2}{E} + \frac{1-\upsilon_i^2}{E_i} \quad (6)$$

Where, β is a constant (β = 1.011 for a Vickers indenter [30]), E_r is the reduced modulus, E and ν are the Young's modulus and Poisson's ratio (0.23 [9]) for the sample, and E_i and ν_i

are the Young's modulus and Poisson's ratio for the indenter (E_i = 1141 GPa and ν_i = 0.07) [31].

3. Results and Discussion

3.1. As-sprayed microstructural analysis

Figs. 3 (a, b) show the scanning electron micrographs of the cross-section of the (a) as-sprayed duplex TBC and the same (b) at high magnification.. Fig. 3a shows the presence of various microstructural defects (i.e. porosities, microcracks, and voids) in the ceramic top coat which are heterogeneously distributed throughout the coating thickness. A high magnification view of the cross-sectional microstructure reveals the presence of globular porosities/voids, interlamellar porosities/cracks, and intralamellar microcracks in the microstructure of the coating as shown in Fig. 3b. The formation of globular porosities is due to incomplete melting or resolidification of molten particles. On the other hand, intralamellar microcracks are formed due to the residual stress relaxation of the individual splats. However, improper bonding between the splats due to difference in temperature of the splats during solidification are responsible for the formation of interlamellar porosities/cracks which is very effective in lowering thermal conductivity and mechanical properties (hardness and Young's modulus) of TBC. . Presence of micro as well as macro-porosities is observed in the microstructure of the duplex thermal barrier coating. The macro-porosities have a negligible effect in lowering the mechanical properties of TBC.

Figs. 4 (a, b) show the scanning electron micrographs of the cross-section of the (a) isothermally aged duplex TBC in air at 1000 °C for 72 h and the same (b) at high

magnification. From Fig. 4a, it is observed that the microstructure of ceramic top coat also contains porosities, microcracks, and voids after high temperature aging. A thermally grown oxide (TGO) layer is formed at the interface between CoNiCrAlY bond coat and YSZ top coat as a result of oxidation of bond coat. Fig. 4b shows the presence of globular porosities/voids, interlamellar porosities/cracks, and intralamellar porosities in the microstructure. A comparison between Fig. 3b and Fig. 4b indicates that the large porosities are unaffected by isothermal aging. On the other hand, bridging in fine microcracks are observed in the microstructure of aged coating which indicates sintering of TBC. The porosity content in ceramic top coat after isothermal aging has been significantly reduced as compared to the as-sprayed duplex TBC. The area fraction of porosities in as-sprayed duplex TBC (plot 1) and the same after isothermal aging in air at 1000 °C for 72 h (plot 2) are calculated by image analysis which is shown in Fig. 5. The area fraction of porosities in as-sprayed duplex TBC is ~ 18.7 % and the same after thermal aging is ~ 8.8 % (cf. Fig. 5). The significant reduction in the area fraction of porosities may be attributed to the sintering effect of the porous TBC.

Figs. 6 (a, b) show the scanning electron micrographs of the cross-section of (a) as-sprayed compositionally graded thermal barrier coating and the same (b) at high magnification. The gradual variation of metallic and ceramic constituents throughout its thickness is observed in compositionally graded TBC (cf. Figure 6a). In addition, there are also presence of various microstructural defects (globular porosities/voids, interlamellar porosities/cracks, and intralamellar porosities) in the microstructure of the compositionally graded TBC(cf. Fig. 6b). Porosities, voids, micro-cracks may be seen in the graded

coating, the details of the same are reported elsewhere [12]. Apart from presence of the microstructural defects, formation of different phases is found in the graded microstructure. The energy dispersive x-ray spectroscopy (EDS) analysis shows that these are oxides of Al (Al_2O_3) and mixed oxides of Co, Ni, Cr, Al as labeled in Fig. 6b. These oxides are formed due to oxidation of metallic elements present in the CoNiCrAlY alloy in a very high temperature environment during plasma spraying.

Figs. 7 (a, b) show the scanning electron micrographs of compositionally graded TBC after (a) isothermal aging at 1000 °C for 72 h and the same (b) at high magnification.. From Fig. 7a, it is observed that a thermally grown oxide (TGO) layer is developed at the bond coat –top coat interface due to oxidation of bond coat. The oxidation of metallic elements present in the graded regions is also observed. The EDS analysis of different phases confirm the presence of Al_2O_3 and mixed oxides of Co, Ni, Cr, Al which are confirmed by X-ray diffraction analysis (cf. Fig. 9).

Fig. 8 shows the X-ray diffraction profiles of top surface of as-sprayed duplex TBC (plot 1) and the same after isothermal aging at 1000 °C for 72 h (plot 2). The presence of non-transformable tetragonal zirconia (t' –ZrO_2) is confirmed from Fig. 8.

Fig. 9 shows the X-ray diffraction profiles of top surface of 100% YSZ (plot 1), 70% YSZ + 30% CoNiCrAlY (plot 3), 50% YSZ + 50% CoNiCrAlY (plot 5), and 30% YSZ + 70% CoNiCrAlY (plot 7) coatings in as-sprayed state and 100% YSZ (plot 2), 70% YSZ + 30% CoNiCrAlY (plot 4), 50% YSZ + 50% CoNiCrAlY (plot 6), and 30% YSZ + 70% CoNiCrAlY (plot 8) coatings after isothermal aging at 1000 °C for 72 h. Comparing plot 1 and plot 2, it may be noted that the there is no separate phase formation other than t' –ZrO_2

in 100% YSZ layer. From plot 3, plot 5, and plot 7, it is observed that apart from formation of t' –ZrO_2 phase, γ –Co phase is also found in the graded layers. With increase in CoNiCrAlY content in the graded layer, the intensity of γ –Co phase increases, whereas, the intensity of t' –ZrO_2 phase decreases. On the other hand, plot 4, plot 6, and plot 8 show the formation of different oxides of Al (Al_2O_3), Co (CoO), Ni and Al ($NiAl_2O_4$), Co and Al ($CoAl_2O_4$), Ni and Cr ($NiCr_2O_4$), and Co and Cr ($CoCr_2O_4$). The formation of various types of oxides depends on the free energy of formation of different oxides as well as the thermodynamic activity of elements for the formation of oxides. It has been reported that Al_2O_3 forms initially followed by formation of other oxides according to their free energy of formation and available chemical potential of the element. Formation of these oxides is found to reduce the kinetics of oxidation of bond coat [12].

3.2. Nanoindentation test

Fig. 10 shows the typical load-displacement curves obtained on the cross-section of the as-sprayed YSZ coating (plot 1) and the same after isothermal aging at 900 °C (plot 2) and 1000 °C (plot 3) for 72 h. From Fig. 10, it is observed that the load-displacement curves depend on the temperature of isothermal aging. Decrease in the penetration depth of the indenter is observed with increase in the aging temperature. The shift in load-displacement curve for the aged surface in the left as compared to as-sprayed one is attributed to the growth of compressive residual stress during isothermal aging.

Fig. 11 shows the Weibull plots of measured (a) reduced modulus and (b) hardness of the as-sprayed YSZ coating and the same after isothermal aging at 900 °C and 1000 °C for 72 h. From the Weibull plots for hardness and Young's modulus, significant data

scattering is observed due to the presence of fine porosities and microcracks in the coating microstructure. These microstructural defects are responsible for lowering of hardness and Youngs modulus as compared to the bulk value. Plot of ln(-ln(1-P)) versus ln E_r is used to obtain the mean value of the reduced modulus and Weibull modulus, where $P = (i - 0.5)/N$ is the probability. Here, i is the rank and N is the total number of measured data. Similarly, ln(-ln(1-P)) versus ln H is plotted to obtain the mean value of the hardness and Weibull modulus. Table 1 summarizes the values of the Young's modulus and Weibull modulus of the as-sprayed YSZ coating and the same after isothermal aging at 900 °C and 1000 °C for 72 h. The Young's modulus value depends on the temperature of aging as observed from the data presented in Table 1. The as-sprayed YSZ coating shows a Young's modulus value of 155 GPa which increases to a value of 170.3 GPa and 183.6 GPa after isothermal aging at 900 °C and 1000 °C, respectively. Similarly, the as-sprayed YSZ coating shows a hardness value of 9.9 GPa which increases to 13.5 GPa and 13.9 GPa due to thermal aging at 900 °C and 1000 °C for 72 h, respectively. Hardness and Young's modulus are affected by the presence of various microstructural defects in the locality of an indentation. The fine porosities (interlamellar porosities) and intralamellar microcracks (cf. 4a) are responsible for decrease in hardness and Young's modulus of the coating. Due to high temperature aging of coatings, the fine porosities and microcracks bridging occurs (cf. 4b) which increases the Young's modulus and hardness of TBC [17, 18]. From Table 1, it is also inferred that the Young's modulus obtained in the present investigation shows a higher value as compared to the reported literature values. The measured Young's modulus values of 93 GPa, 100 GPa, and 94 GPa are obtained for an indentation depth of ~ 2000 nm

whereas a depth up to ~ 300 nm is obtained in the present study. Similarly, Thompson *et al.* [18] reported a Young's modulus value of 144.5 GPa with a maximum indentation load of 100 mN. As the indentation depth is directly related to the applied indentation load, hence, the reported data on the hardness and Young's modulous are probably taken at a higher applied load. The observed differences between the reported literature values and the same obtained in the present investigation are mainly attributed to the use of lower indentation load in the present study and the phenomenon of "*Indentation size effect*" [32]. The hardness and Young's modulous value measured using the similar level of load for comparison are not however, available in the literatures. Fig. 12 shows the Young's modulus distribution in the as-sprayed compositionally graded TBC. From Fig. 12, it can be seen that the top layer (100% YSZ) shows lower value of Young's modulus as compared to the underlying surface layers towards the bond coat –top coat interface. The Young's modulus value in the near surface region of the TBC coated surface (near surface region) ranges from 58 GPa to 150 GPa measured at a maximum indentation load of 8 mN. The wide variation in Young's modulus distribution in the coated zone is attributed to the presence of fine porosities and microcracks distributed non-uniformly on the surface. In the graded layer, Young's modulus is found to vary from 151 to 224 GPa. The inhomogeneous Young's modulus distribution in the graded regions is attributed to the random distribution of different phases in the graded layers and presence of different microstructural defects. The reported Young's modulus values of YSZ are 80 GPa [19], 100 GPa [34] and 94 GPa [35] measured up to an indentation depth of ~ 2000 nm, 96 GPa [16] and 144 GPa [18] at an indentation load of 100 mN. The reported values of Young's modulus of CoNiCrAlY

bond coat and Al_2O_3 scales are~155 GPa measured up to an indentation depth of ~ 2000 nm [35] and 250 GPa measured at an indentation load of 100 mN after isothermal aging at 1150 °C up to 10 h, respectively [19]. Taking into account the reported values and the observed values of Young's modulus, it is assumed that Young's modulus ranging from 187 GPa to 224 GPa may be contributed by Al_2O_3 scales. The observed difference between the reported and the calculated values of Young's modulus of Al_2O_3 scale may be attributed to the presence of microstructural defects as well as contribution from oxides other than Al_2O_3 (cf. Fig. 6b). Comparing the reported values of Young's modulus and the Young's modulus values obtained in the present investigation, it is observed that the Young's modulus values ranging from 150 GPa to 187 GPa may be contributed by the CoNiCrAlY phase. In a similar manner, Young's modulus values ranging from 58 GPa to 150 GPa may be contributed by the YSZ phase. From Fig. 12, it is observed that the Young's modulus increases with increase in CoNrAlY content in the graded layers which is attributed to the presence of metallic CoNiCrAlY bond coat which has no intralamellar cracks in it (cf. Fig. 6b).

Fig. 13 shows the Young's modulus distribution throughout the graded TBC after isothermal aging at 900 °C for 72 h. From Fig. 13, it is evident that the Young's modulus is increased from as-sprayed state to the isothermally aged state. Increase in the Young's modulus is due to oxidation of CoNiCrAlY and formation of oxides with a higher Young's modulus. The increase in Young's modulus with isothermal aging at 900 °C for 72 h may also be attributed to the densification of the microstructure. As the mechanical properties (hardness and Young's modulus) depends on the local microstructural defects near

indentation, the closure of fine porosities (interlamellar porosities) and intralamellar microcracks due to high temperature sintering leads to increase in Young's modulus. It is reported that the Young's modulus of Al_2O_3 scale is increased from 250 GPa to 350 GPa due to thermal aging at 1150 °C and also increases with increase in time of aging [19]. Hence, the Young's modulus values ranging from 193 GPa to 212 GPa is contributed by the Al_2O_3 rich oxide scales formed in the graded regions. The difference between the observed and the reported Young's modulus values may be attributed to the formation and growth other complex oxides (cf. Fig. 9) as well as presence of microcracks and fine porosities in the microstructure of the graded TBC. It is reported that the observed difference between the Young's modulus of TGO (preferably Al_2O_3) and the bulk Al_2O_3 is due to the presence of fine microcracks in TGO [19]. It is also reported that the Young's modulus of CoNiCrAlY is increased from 134-154 GPa to 202 - 216 GPa due to thermal aging at 1100 °C for 24 h which further increases with increase in time [36]. Hence, the Young's modulus ranging from 174 to 193 GPa is contributed by the presence of CoNiCrAlY phase. It is also reported that Young's modulus of YSZ varies with time from 144 GPa to 177 GPa due to thermal aging at 1100 °C [23] and 135 GPa to 170 GPa due to thermal aging at 1150 °C [19]. Taking into account the presence of microstructural defects present in the locality of an indentation and the use of lower indentation load, it is assumed that the Young's modulus varying from 61 GPa to 174 GPa is contributed from YSZ phase. The lower value of Young's modulus in YSZ coated zone as compared to the same reported in the literature is due to the presence of fine microcracks in the coating cross-section (cf. Fig. 7b). Fig. 14 shows the Young's modulus distribution throughout the graded TBC after

isothermal aging at 1000 °C for 72 h. From Fig. 14, it is evident that the Young's modulus is significantly increased due to increase in the temperature of aging. Taking into account the reported values of Young's modulus of aged Al_2O_3, CoNiCrAlY, and YSZ phases and the values obtained for graded TBC thermally aged at 900 °C for 72 h, it is thus assumed that the Young's modulus varying from 234 GPa to 264 GPa is contributed by Al_2O_3, the Young's modulus varying from 206 GPa to 234 GPa is contributed by CoNiCrAlY, and the Young's modulus varying from 37 GPa to 206 GPa is contributed by YSZ after isothermal aging at 1000 °C for 72 h. The increase in the Young's modulus value of YSZ may be attributed to the sealing of fine microcracks or porosities due to thermal aging. The use of lower indentation load and presence of different phases (Fig. 7b) as well as microstructural defects (Fig. 7b) are the reasons behind the difference between the reported values and the measured values obtained in the presence investigation From Fig. 8 to Fig. 10, it may be inferred that the Young's modulus in the graded coating increases with increase in percentage of CoNiCrAlY in the graded layers, which is indeed beneficial in reducing residual thermal stress of the coating, especially after thermal aging.

Table 2 shows the variation in the Young's modulus values measured in as-sprayed graded top coat and the same isothermally aged at 900 °C and 1000 °C for 72 h determined by nanoindentation test. From Table 2, it is evident that the Young's modulus in as-sprayed graded top coat varies between 59 GPa to 206 GPa. With increase in the temperature of isothermal aging, the Young's modulus varies from 61 GPa to 212 GPa at 900 °C and 38 GPa to 262 GPa at 1000 °C. The scattering in the Young's modulus value is due to the presence of different types of microstructural defects as well as formation of different

oxides due to the presence of CoNiCrAlY alloy in the graded TBC. Similar variation in the data obtained for hardness is also found.

Table 3 summarizes the modulus of resilience and plasticity index of as-sprayed duplex TBC and the same after isothermal aging at 900 °C and 1000 °C for 72 h, respectively. The modulus of resilience of duplex TBC increases from 35 MPa (in as-sprayed state) to 68 MPa and 58 MPa due to isothermal aging at 900 °C and 1000 °C, respectively, for 72 h. Hence, it is apparent that the high temperature treatment of duplex TBC increases the resistance to plastic deformation. From Table 3, it is apparent that no trend in modulus of resilience is observed which may be attributed to the heterogeneous distribution of fine microcracks and porosities in the coating cross-section and the use of lower indentation load. The nanoindenation gives the local properties which are directly related to the presence of volume defects in the vicinity or under the indenter tip. Hence, decrease in defects density due to isothermal aging increases the modulus of resilience. However, there is a decrease in plasticity index with thermal aging which decrease with increase in aging temperature.

Table 4 shows the modulus of resilience and plasticity index of as-sprayed graded TBC and the same after isothermal aging at 900 °C and 1000 °C for 72 h determined by nanoindentation technique. From Table 4, it is observed that the modulus of resilience in as-sprayed 100% YSZ layer, 70% YSZ + 30% CoNiCrAlY, 50% YSZ + 50% CoNiCrAlY, and 30% YSZ + 70% CoNiCrAlY coatings are 35 MPa, 24 MPa, 13 MPa, and 34 MPa, respectively. The plasticity index in as-sprayed 100% YSZ layer, 70% YSZ + 30% CoNiCrAlY, 50% YSZ + 50% CoNiCrAlY, and 30% YSZ + 70% CoNiCrAlY coatings are

50.5%, 54.6%, 70.9%, and 66.4%, respectively. The composite layers show increase in plasticity index as compared to the 100% YSZ coating. However, the modulus of resilience in isothermally aged 100% YSZ, 70% YSZ + 30% CoNiCrAlY, 50% YSZ + 50% CoNiCrAlY, and 30% YSZ + 70% CoNiCrAlY coatings, at 900 °C for 72 h, are 59 MPa, 32 MPa, 35 MPa, and 40 MPa, respectively. The modulus of resilience decreases due to addition of CoNiCrAlY in the coating, however, the variation of modulus of resilience by varying CoNiCrAlY content does not follow any specific trend. Hence, it is concluded that due to the presence of CoNiCrAlY content in the graded layer, the resistance to plastic deformation decreases. On the other hand, the plasticity index in the graded layers increases with addition of CoNiCrAlY content, though the variation of plasticity index with increase in CoNiCrAlY content does not follow any specific trend. Hence, though there is reduced elastic recovery due to the presence of metallic content in the graded layer, however, the effect of metallic content on the elastic recovery does not follow any trend. Presence of localized microstructural defects in aged coatings contributes to the nonlinear behavior of data. With further increase in isothermal aging temperature to 1000 °C, it is observed that the modulus of resilience in 100% YSZ, 70% YSZ + 30% CoNiCrAlY, 50% YSZ + 50% CoNiCrAlY, and 30% YSZ + 70% CoNiCrAlY layers are 58 MPa, 50 MPa, 38 MPa, and 37 MPa, respectively. The modulus of resilience decreases with increase in CoNiCrAlY content in the graded layers. The observation suggests that the graded layer with increasing CoNiCrAlY content shows a lower resistance to plastic deformation. On the other hand, the plasticity index in the graded layers increases with increase in CoNiCrAlY content which suggests that the graded layer with a higher CoNiCrAlY content shows a lower elastic

recovery. Comparing the as-sprayed graded TBC and compositionally graded TBC after isothermal aging at 900 °C and 1000 °C for 72 h, it may be inferred that the modulus of resilience increases due to isothermal aging, i.e. the coating becomes more resistant to plastic deformation under the influence of isothermal aging.

4. Conclusions

In the present study, the hardness and Young's modulus of the duplex as well as compositionally graded thermal barrier coating have been measured in details both in as-sprayed state and after isothermal aging at temperatures ranging from 900 °C to 1000 °C for 72 h. From the detailed investigations, the following conclusions may be drawn:

1. Various types of porosities and cracks are present in the microstructure of both the duplex and graded YSZ based thermal barrier coating. The extent of porosities and defect contents are found to decrease due to isothermal aging at high temperature.
2. Nanoindentation of as-sprayed duplex TBC and isothermally exposed duplex TBC suggests that the Young's modulus increases from 155 GPa in as-sprayed state to 170 GPa and 183 GPa due to isothermal aging at 900 °C and 1000 °C (for 72 h), respectively. The hardness increases from 9.9 GPa in as-sprayed state to 13.5 GPa and 13.9 GPa after isothermal aging at 900 °C and 1000 °C (for 72 h), respectively.
3. The cross-sectional modulus mapping in as-sprayed compositionally graded coating and aged compositionally graded coating shows variation of Young's modulus depending on percentage of CoNiCrAlY in the coating layers. The Young's modulus was found to increase with depth from surface in as-sprayed state as well as after thermal aging at high temperature.

4. The resilience and plasticity index (%) are calculated for both the duplex and graded TBC in as-sprayed condition and after isothermal aging. It is observed that both for duplex and graded coating, resilience increases and plasticity index decreases due to thermal aging. Furthermore, the resilience decreases and plasticity index increases with addition of CoNiCrAlY content in the coating.

Acknowledgements

The partial financial support from the Department of Science and Technology (DST), New Delhi, Council of Scientific and Industrial Research, New Delhi and Indian Space Research Organization (ISRO) are gratefully acknowledged.

References

1. W. R Chen, X. Wu, B. R. Marple, P. C. Patnaik, Oxidation and crack nucleation/growth in an air-plasma-sprayed thermal barrier coating with NiCrAlY bond coat, Surf. Coat. Technol. 197 (2005) 109-115.

2. M. Nejati, M. R. Rahimipour, I. Mobasherpourn, Evaluation of hot corrosion behavior of CSZ, CSZ/micro Al_2O_3 and CSZ/nano Al_2O_3 plasma sprayed thermal barrier coatings, Ceram. Int. 40 (2014) 4579–4590.

3. M. R. Loghman-Estarki, R. S. Razavi, H. Edris, M. Pourbafrany, H. Jamali, R. Ghasemi, Life time of new SYSZ thermal barrier coatings produced by plasma

spraying method under thermal shock test and high temperature treatment, Ceram. Int. 40 (2014) 1405–1414.

4. A. Rico, J. Gómez-García, C.J. Múnez, P. Poza, V. Utrilla, Mechanical properties of thermal barrier coatings after isothermal oxidation: Depth sensing indentation analysis Surf. Coat. Technol. 203 (2009) 2307-2314.

5. A. Bolcavage, A. Feuerstein, J. Foster, P. Moore, Thermal shock testing of thermal barrier coating/bondcoat systems, J. Mater. Eng. Perform. 30 (2004) 389-397.

6. W.Y. Lee, D.P. Stinton, C.C. Berndt, F. Erdogan, Y.D. Lee, Z. Mutasim, Concept of functionally graded materials for advanced thermal barrier coating applications: A review, J. Am. Ceram. Soc. 79 (1996) 3003-3012.

7. A.S. Demirkiran, E. Avci, Evaluation of Functionally Gradient Coatings Produced by Plasma-Spray Technique, Surf. Coat. Technol. 116 (1999) 292-295.

8. A Kawasaki, R Watanabe, Thermal fracture behavior of metal/ceramic functionally graded materials, Eng. Fract. Mech. 69 (2002) 1713-1728.

9. K.A. Khor, Y.W. Zu, Effects of residual stress on the performance of plasma sprayed functionally graded ZrO_2: NiCoCrAlY coatings, Mater. Sci. Eng., A 277 (2000) 64-76.

10. K.A. Khor, Y.W. Zu, Thermal properties of plasma-sprayed functionally graded thermal barrier coatings, Thin Solid Films 372 (2000) 104-113.

11. S. Nath, I. Manna, J. Dutta Majumdar, Kinetics and mechanism of isothermal oxidation of compositionally graded yttria stabilized zirconia (YSZ) based thermal barrier coating, Corros. Sci. (2014) DOI: 10.1016/j.corsci.2014.06.050.

12. S. Nath, I. Manna, J. Dutta Majumdar, Compositionally graded thermal barrier coating by hybrid thermal spraying route and its non-isothermal oxidation behavior, J. Therm. Spray Technol. 22 (2013) 901–917

13. R. Ghasemin, R. Shoja-Razavi, R. Mozafarinia, H. Jamali, Comparison of microstructure and mechanical properties of plasma-sprayed nanostructured and conventional yttria stabilized zirconia thermal barrier coatings, Ceram. Int. 39 (2013) 8805–8813.

14. N. Zotov, M. Bartsch, G. Eggeler, Thermal barrier coating systems - analysis of nanoindentation curves, Surf. Coat. Technol. 203 (2009) 2064–2072.

15. S. Guo, Y. Kagawa, Effect of thermal exposure on hardness and Young's modulus of EB-PVD yttria-partially-stabilized zirconia thermal barrier coatings, Ceram. Int. 32 (2006) 263–270.

16. A. Afrasiabi, A. Kobayashi, Hot corrosion control in plasma sprayed YSZ coating by alumina layer with evaluation of microstrcuture and nanoindentation data (H, E), Vacuum 88 (2013) 103-107.

17. M. Alfano, G. Di Girolamo, L. Pagnotta, D. Sun, J. Zekonyte, R. J. K. Wood, The influence of high temperature sintering on microstructure and mechanical properties of free standing APS CeO_2-Y_2O_3-ZrO_2 coatings, J. Mater. Sci. 45 (2010) 2662-2669.

18. J.A. Thompson, T.W. Clyne, The effect of heat treatment on the stiffness of zirconia top coats in plasma-sprayed TBCs, Acta Mater. 49 (2001) 1565-1575.

19. S. Guo, Y. Kagawa, Young's moduli of zirconia top-coat and thermally grown oxide in a plasma-sprayed thermal barrier coating system, Scr. Mater. 50 (2004) 1401–1406.

20. A. Diaz-Parralejo, A.L. Ortiz, R. Caruso, Effect of sintering temperature on the microstructure and mechanical properties of ZrO_2-3 mol% Y_2O_3 sol–gel films, Ceram. Int. 36 (2010) 2281–2286.

21. Y. Bai, K.Liu, Z. H. Wen, J. J. Tang, L. Zhao, Z. H. Han, The influence of particle in-flight properties on the microstructure of coatings deposited by the supersonic atmospheric plasma spraying, Ceram. Int. 39 (2013) 8549–8553.

22. Y. Baia, J. J. Tang, Y. M. Qu, S. Q. Ma, C. H. Ding, J. F. Yang, L. Yu, Z. H. Han, Influence of original powders on the microstructure and properties of thermal barrier coatings deposited by supersonic atmospheric plasma spraying, Part I: Microstructure, Ceram. Int. 39 (2013) 5113–5124.

23. B. Siebert, C. Funke, R. Vaβen, D. Stover, Changes in porosity and Young's modulus due to sintering of plasma sprayed thermal barrier coatings, J. Mater. Process. Technol. 92-93 (1999) 217-223.

24. A. Dey, R. U. Rani, H. K. Thota, A. K. Sharma, P. Bandyopadhyay, A. K. Mukhopadhyay, Microstructural, corrosion and nanomechanical behaviour of ceramic coatings developed on magnesium AZ31 alloy by micro arc oxidation, Ceram. Int. 39 (2013) 3313–3320.

25. A. Dey, A. K. Mukhopadhyay, S. Gangadharan, M.K. Sinha, D. Basu, N. R. Bandyopadhyay, Nanoindentation study of microplasma sprayed hydroxyapatite coating, Ceram. Int. 35 (2009) 2295–2304.

26. B. Jang, H. Matsubara, Influence of porosity on hardness and Young's modulus of nanoporous EB-PVD TBCs by nanoindentation, Mater. Lett. 59 (2005) 3462–3466.

27. S.T. Aruna, B. Arul Paligan, N. Balaji, V. Praveen Kumar, Properties of plasma sprayed yttria stabilized zirconia thermal barrier coating prepared from co-precipitation synthesized powder, Ceram. Int. 40 (2014) 11157–11162.

28. W.C. Oliver, G.M. Pharr, An improved technique for determining hardness and elastic modulus using load and displacement sensing indentation experiments, J. Mater. Res. 7 (1992) 1564–1583.

29. I. N. Sneddon, The relation between load and penetration in the axisymmetric boussinesq problem for punch of arbitrary profile, Int. J. Eng. Sci. 3 (1965) 47–57.

30. R.B. King, Elastic analysis of some push problems for a layered medium, Int. J. Solids Struct. 23 (1987) 1657–1664.

31. G. Simmons, H. Wang, Single Crystal Elastic Constants and Calculated Aggregate Properties: A Handbook, MIT Press, Cambridge, MA, 1971.

32. Yu. V. Milman, A. A. Golubenko, S. N. Dub, Indentation size effect in nanohardness, Acta Mater. 59 (2011) 7480–7487.

33. J. Y. Kwon, J. H. Lee, H. C. Kim, Y.G. Jung, U. Paik, K.S. Lee, Effect of thermal fatigue on mechanical characteristics and contact damage of zirconia-based thermal barrier coatings with HVOF sprayed bond coat, Mater. Sci. Eng., A 429 (2006) 173-180.

34. H. Jang, D. Park, Y. Jung, J. Jang, S. Choi, U.Paik, Mechanical characterization and thermal behavior of HVOF-sprayed bond coat in thermal barrier coatings (TBCs), Surf. Coat. Technol. 200 (2006) 4355 – 4362.

35. J. Kwon, J. Lee, Y. Jung, U. Paik, Effect of bond coat nature and thickness on mechanical characteristic and contact damage of zirconia-based thermal barrier coatings, Surf. Coat. Technol. 201 (2006) 3483–3490.

36. G. Di Girolamo, M. Alfano, L. Pagnotta, A. Taurino, J. Zekonyte, and R.J.K. Wood, On the early stage isothermal oxidation of APS CoNiCrAlY Coatings, J. Mater. Eng. Perform. 21 (2012) 1989-1997.

List of Figures

List of Tables

Table 4 Modulus of resilience and plasticity index of as-sprayed graded TBC and the same after isothermal exposure at 900 °C and 1000 °C for 72 h measured by nanoindentation technique.

Table 1
Young's modulus and hardness values of as-sprayed YSZ top coat and the same after isothermal exposure at 900 °C and 1000 °C for 72 h measured by nanoindentation technique.

Sample	Young's modulus, GPa	Weibull modulus	Hardness, GPa	Weibull modulus
As-sprayed YSZ top coat	155[a], 93[b], 144.5[c], 100[d], 94[e]	3.45	9.9[a], 5.8[b], 8.7[c], 3.5-5.5[d], 4.2[e]	1.82
Isothermal exposure of YSZ top coat at 900 °C for 72 h	170.3 [a]	7.93	13.5 [a]	2.94
Isothermal exposure of YSZ top coat at 1000 °C for 72 h	183.6 [a]	6.94	13.9 [a]	4.03

a- Present study; b- [33]; c- [18]; d- [34]; e- [35]

Table 2
Young's modulus and hardness values of as-sprayed graded TBC and the same after isothermal aging at 900 °C and 1000 °C for 72 h measured by nanoindentation technique.

Sample	Young's modulus, GPa	Hardness, GPa
As-sprayed graded TBC	59 - 206	4.5 – 15.2
Isothermal aging of graded TBC at 900 °C for 72 h	61 - 212	2.6 – 17.7
Isothermal aging of graded TBC at 1000 °C for 72 h	38 - 262	1.2 – 19.1

Table 3
Modulus of resilience and plasticity index in as-sprayed YSZ top coat and the same after isothermal aging at 900 °C and 1000 °C for 72 h measured by nanoindentation technique.

Sample	Modulus of resilience, MPa	Plasticity index (%)
As- sprayed YSZ top coat	35	50.5
Isothermal aging of YSZ top coat at 900 °C for 72 h	68	42
Isothermal aging of YSZ top coat at 1000 °C for 72 h	58	39.5

Table 4
Modulus of resilience and plasticity index of as-sprayed graded TBC and the same after isothermal aging at 900 °C and 1000 °C for 72 h measured by nanoindentation technique.

Sample	As-sprayed graded TBC		Graded TBC after isothermal aging at 900 °C for 72 h		Graded TBC after isothermal aging at 1000 °C for 72 h	
	Modulus of resilience, MPa	Plasticity index (%)	Modulus of resilience, MPa	Plasticity index (%)	Modulus of resilience, MPa	Plasticity index (%)
100% YSZ	35	50.5	59	41.9	58	39.6
70% YSZ + 30% CoNiCrAlY	24	54.6	32	60.7	50	52.2
50% YSZ + 50% CoNiCrAlY	13	70.9	35	50.3	38	60.2
30% YSZ + 70% CoNiCrAlY	34	66.4	40	55	37	57.8

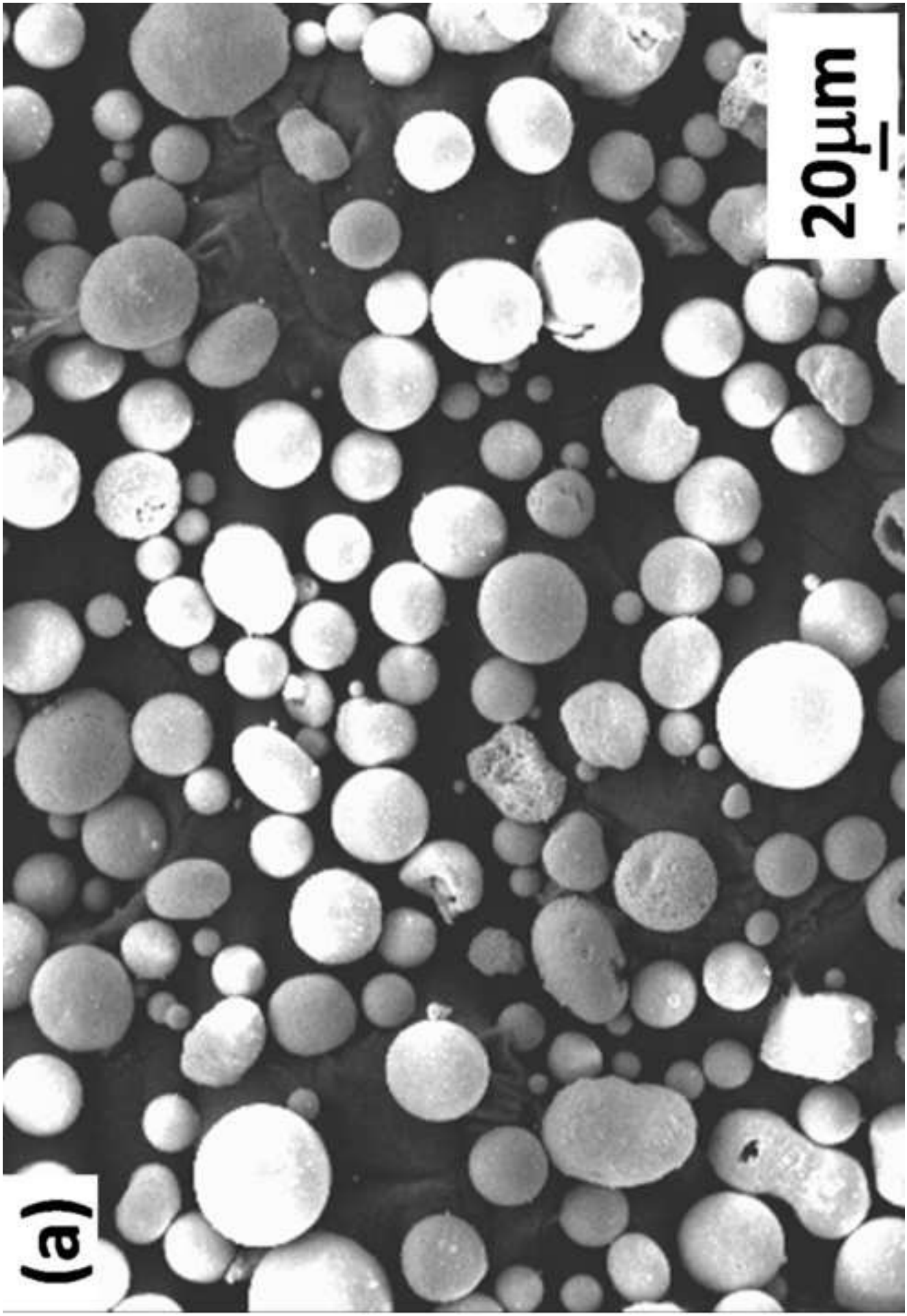

Figure-1a

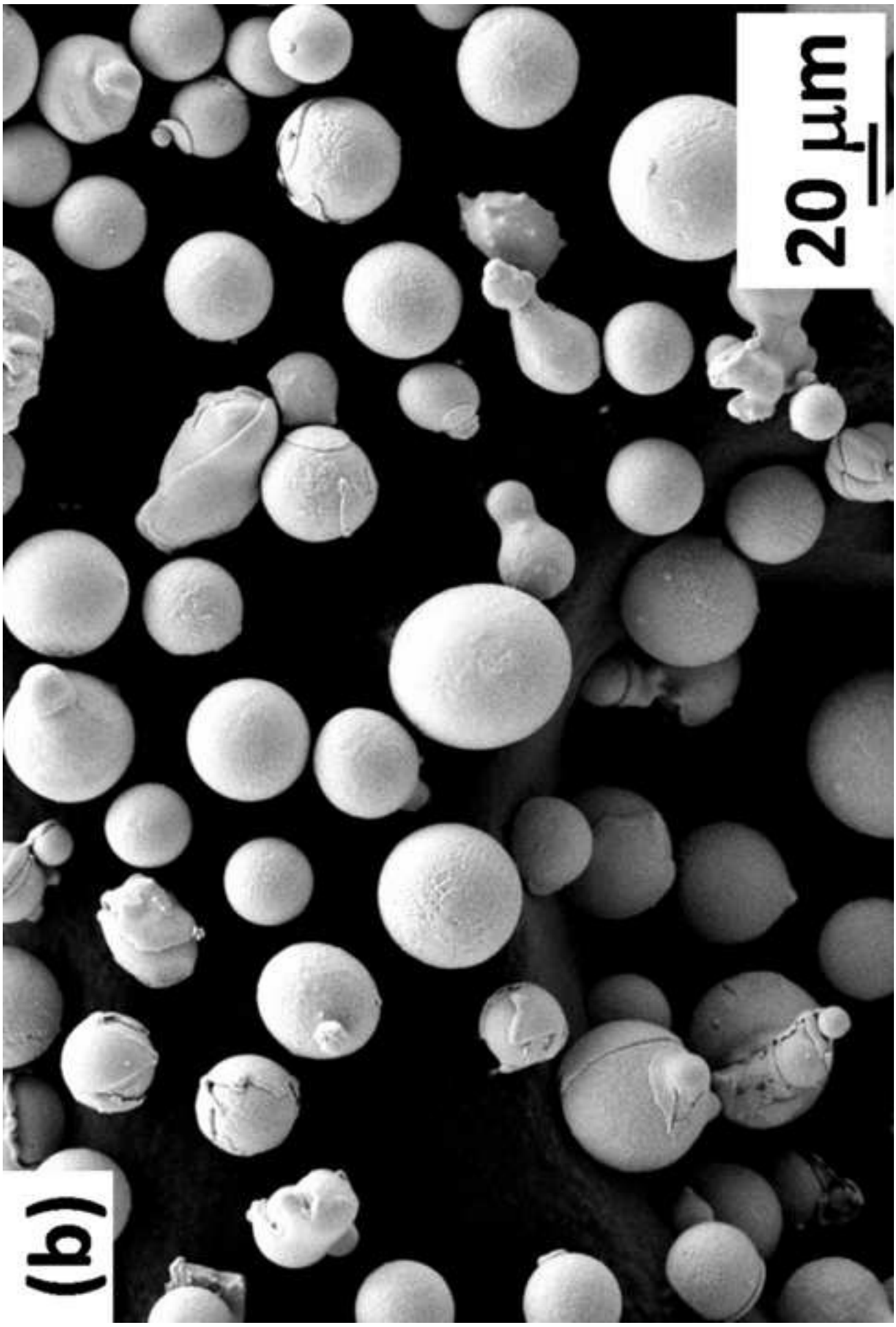

Figure-1b

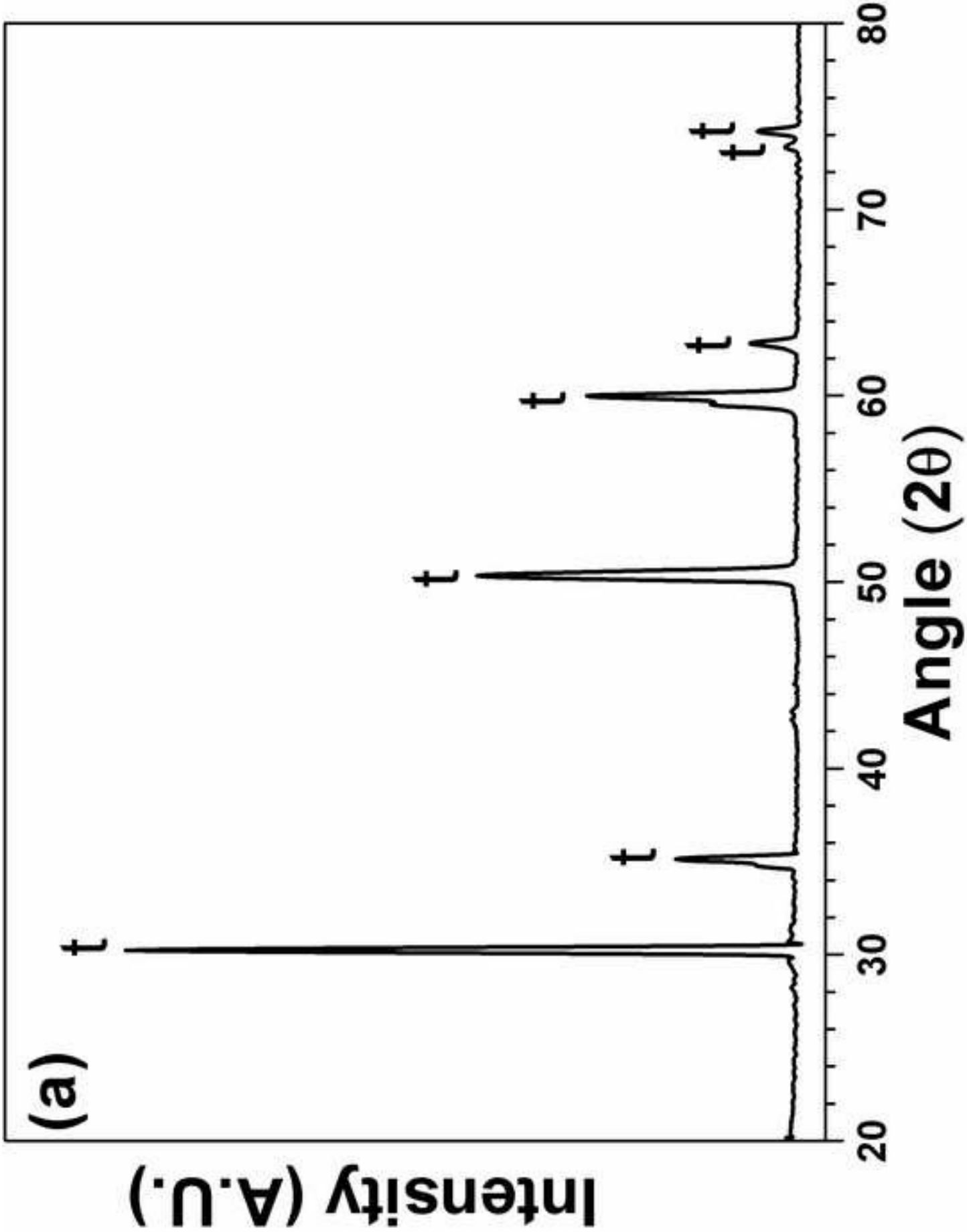

Figure-2a

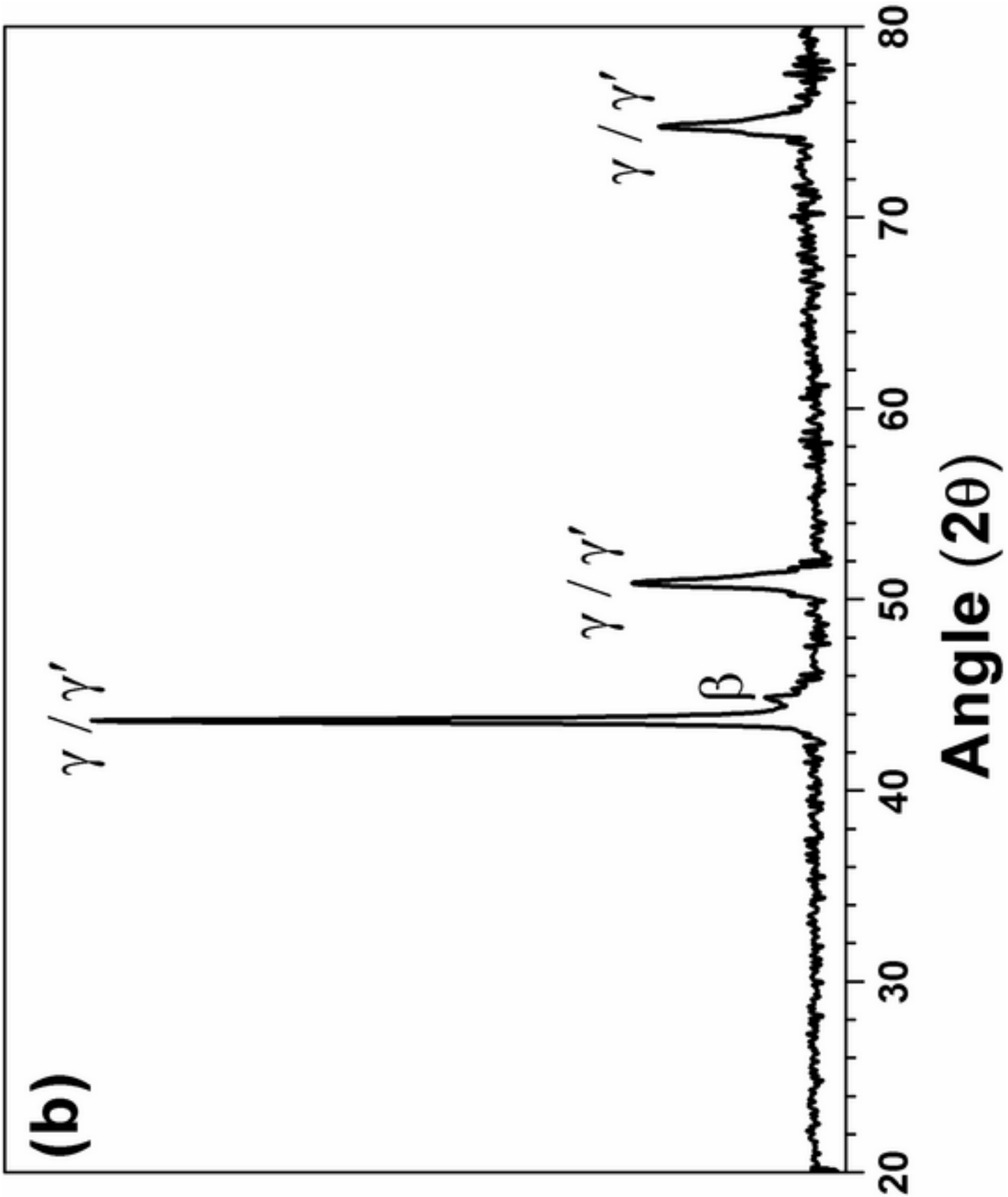

Figure-2b

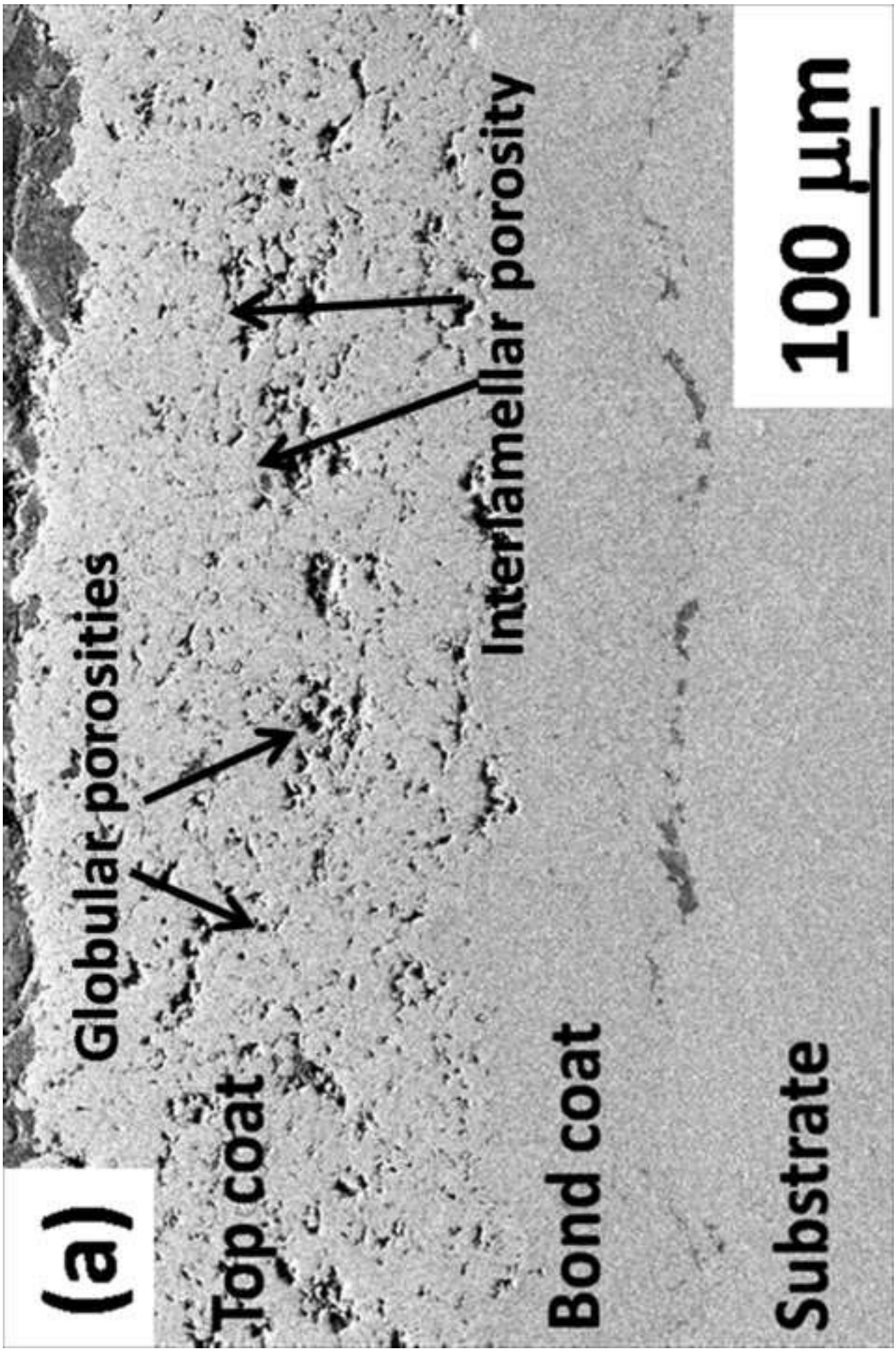
(a)
Globular porosities
Top coat
Interlamellar porosity
Bond coat
Substrate
100 µm

Figure-3a

Figure-3b

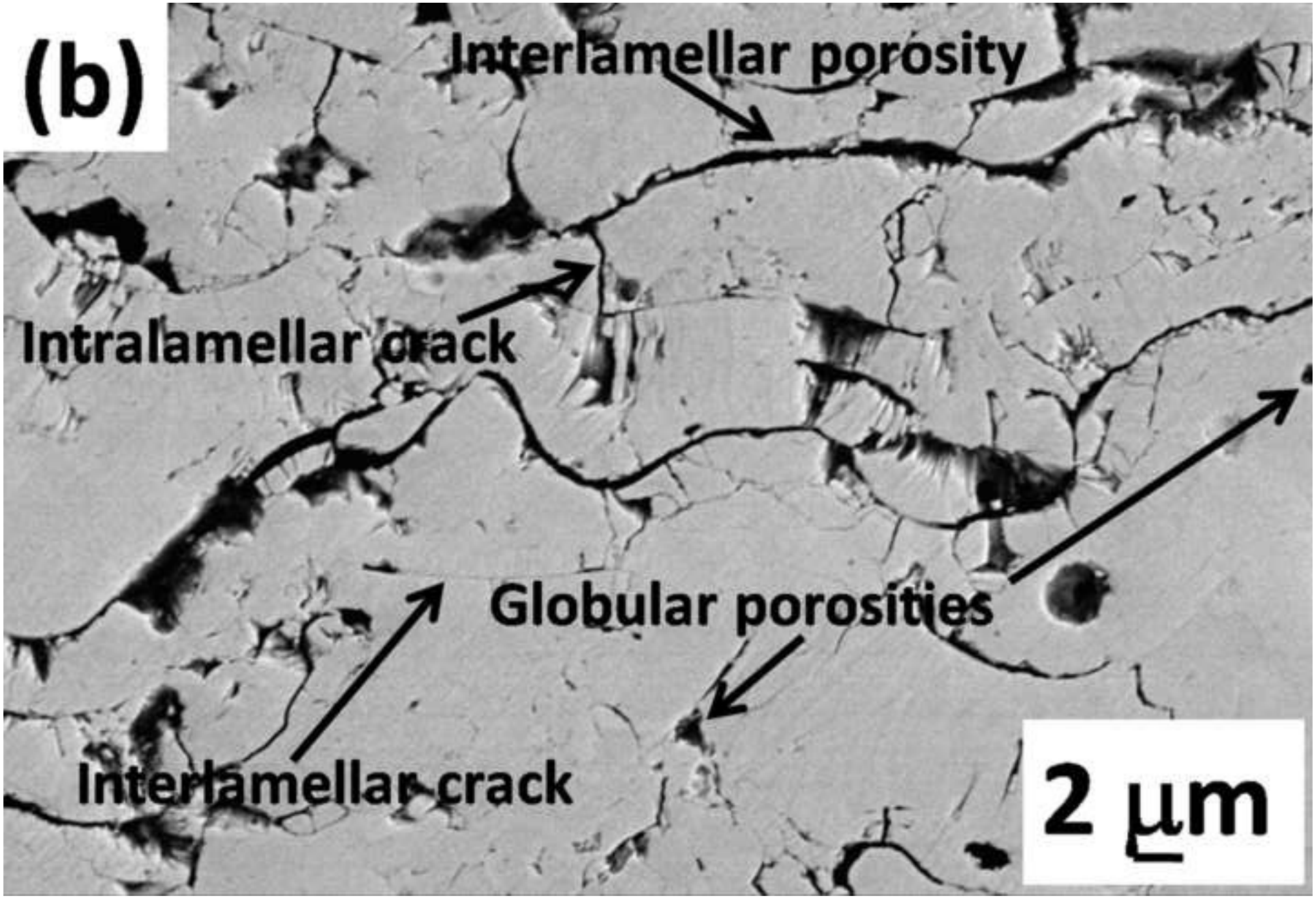

Figure-4a

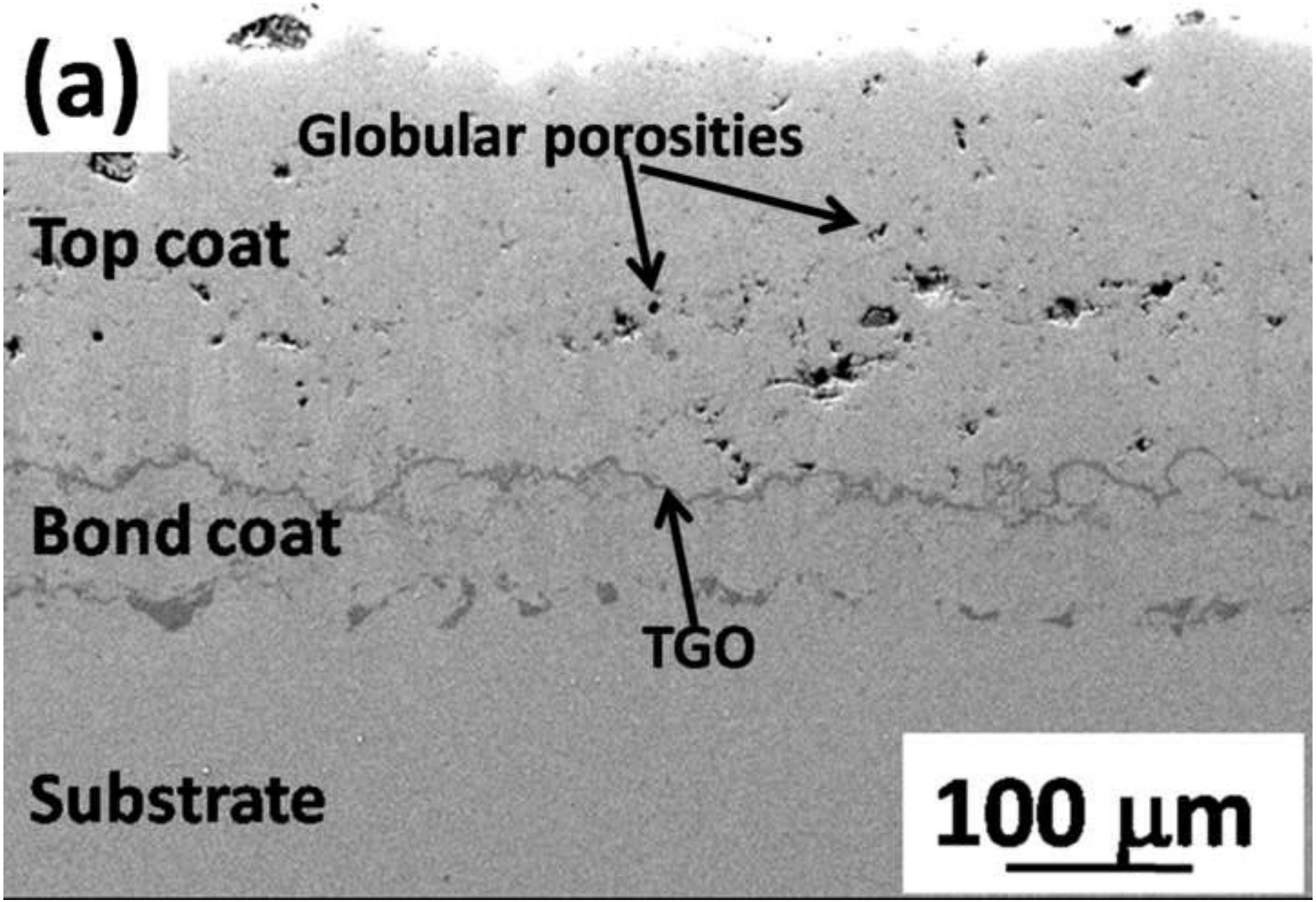

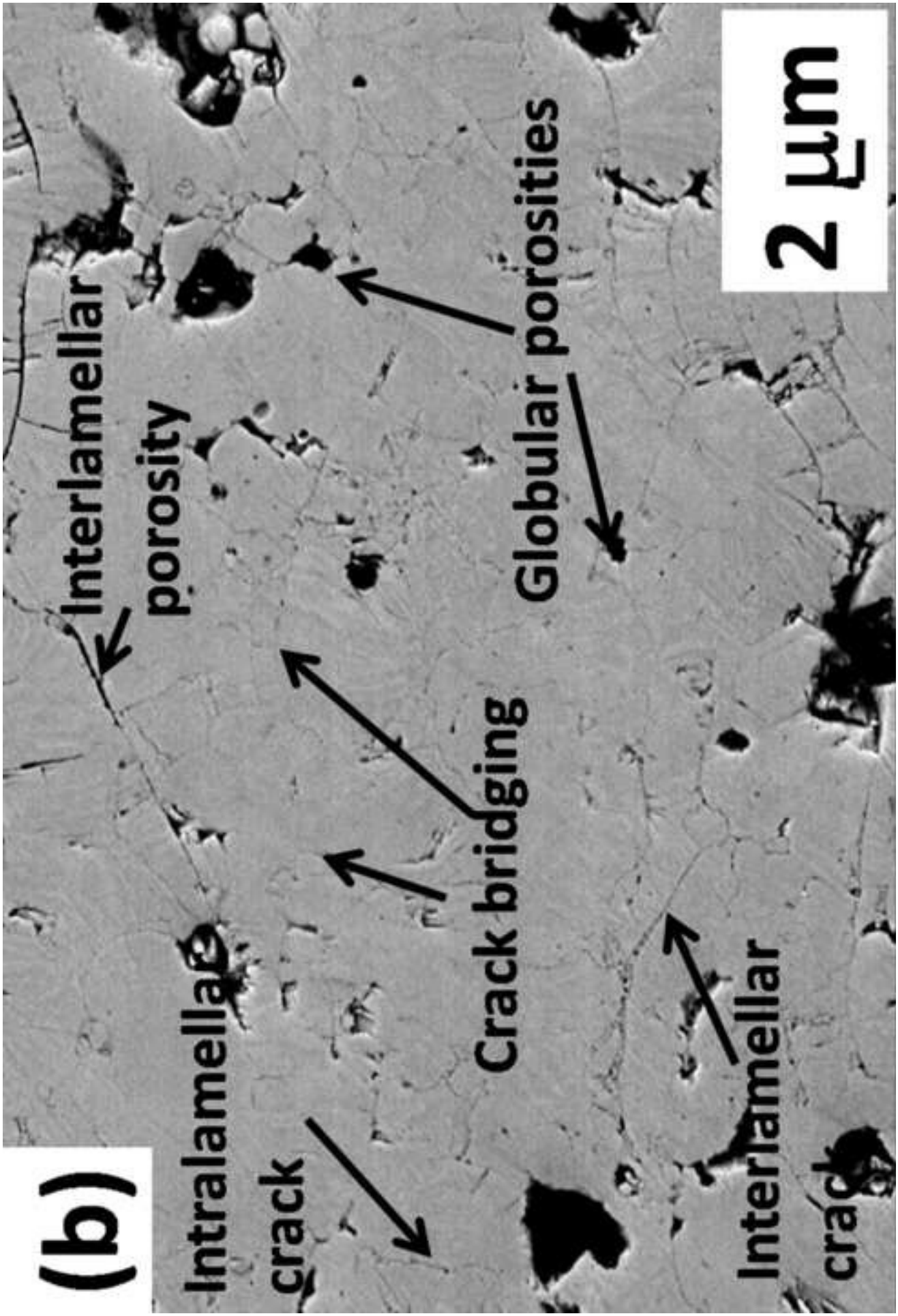

Figure-4b

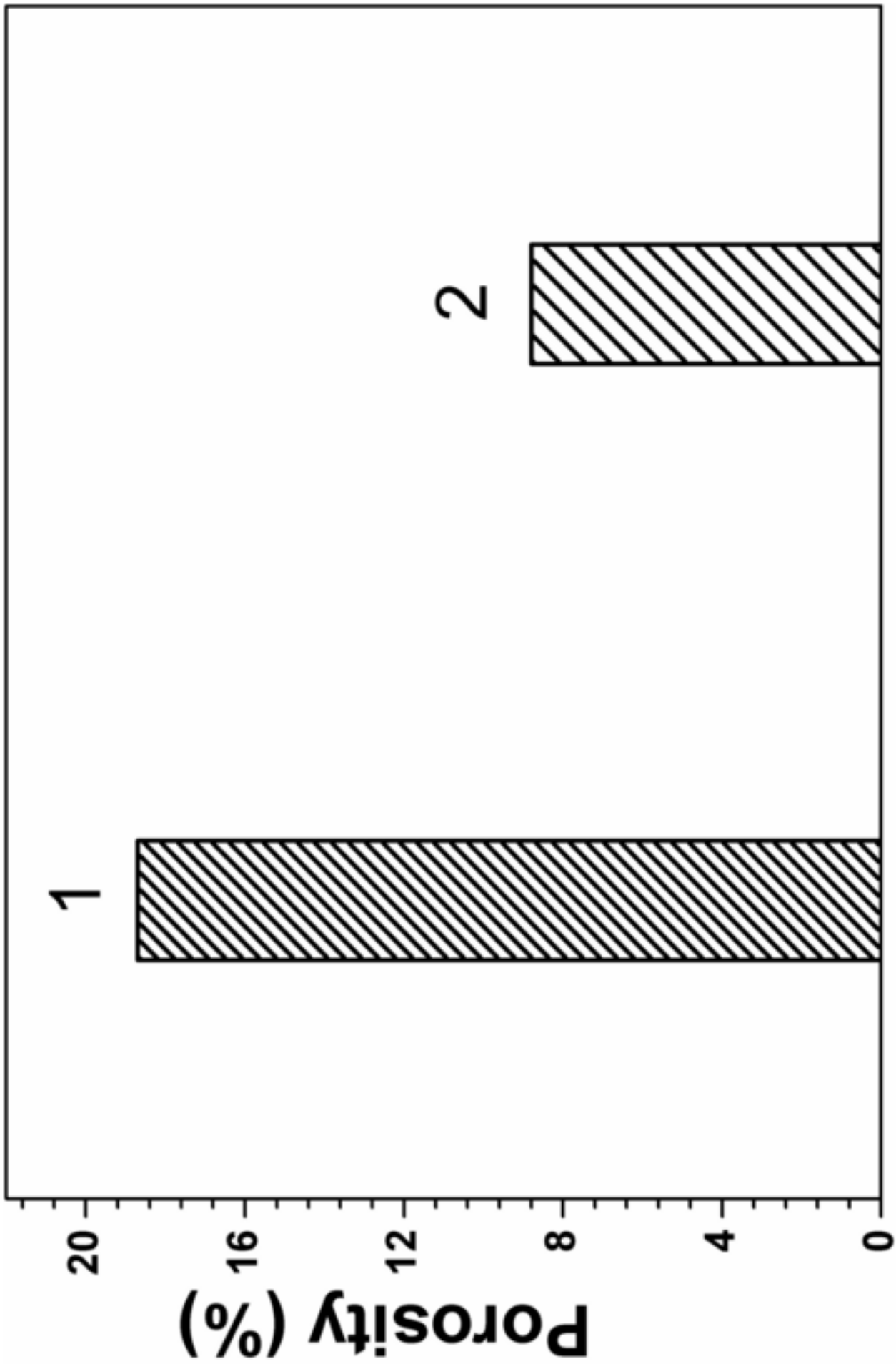

Figure-5

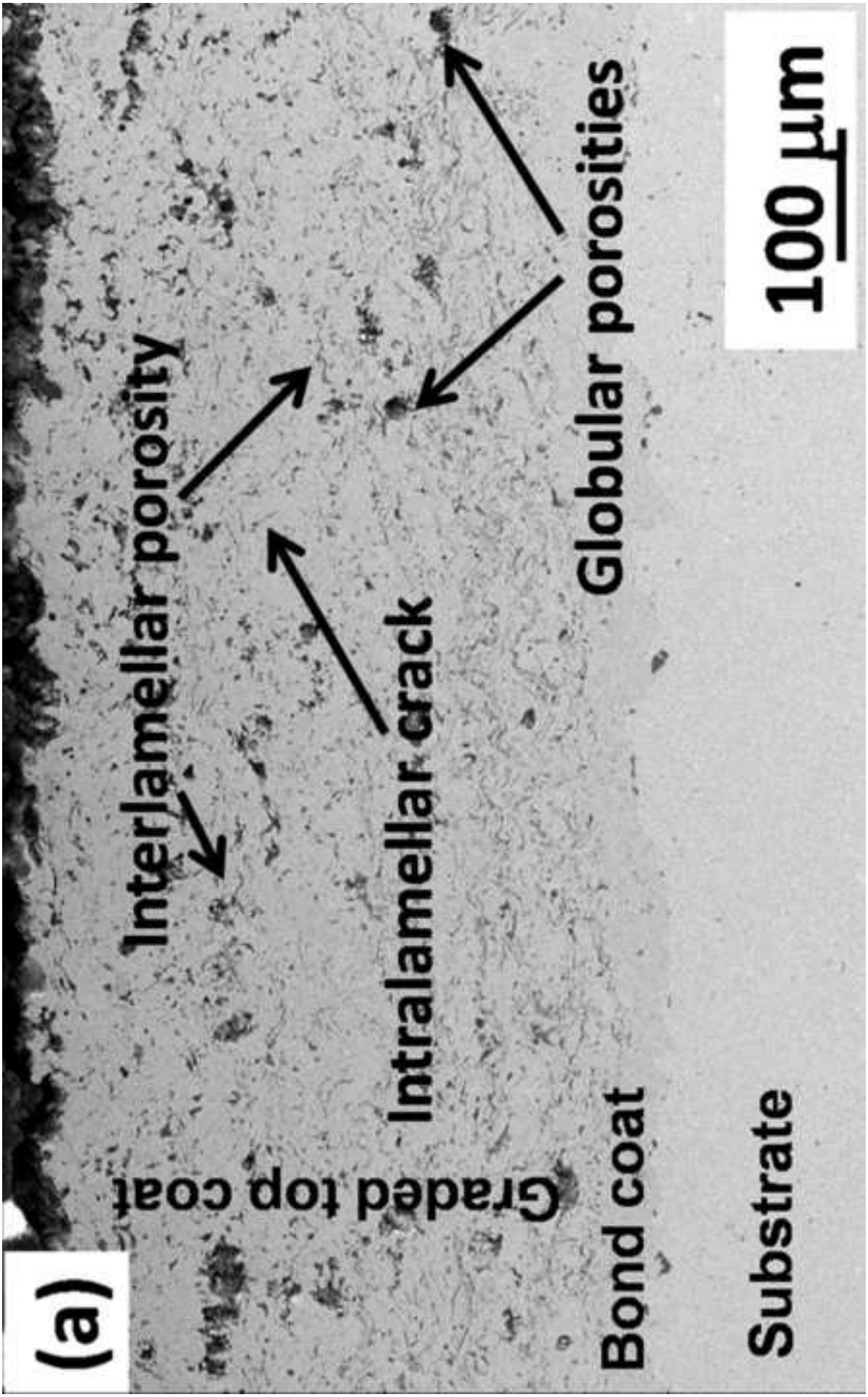
(a)
Graded top coat
Bond coat
Substrate
Interlamellar porosity
Intralamellar crack
Globular porosities
100 µm

Figure-6a

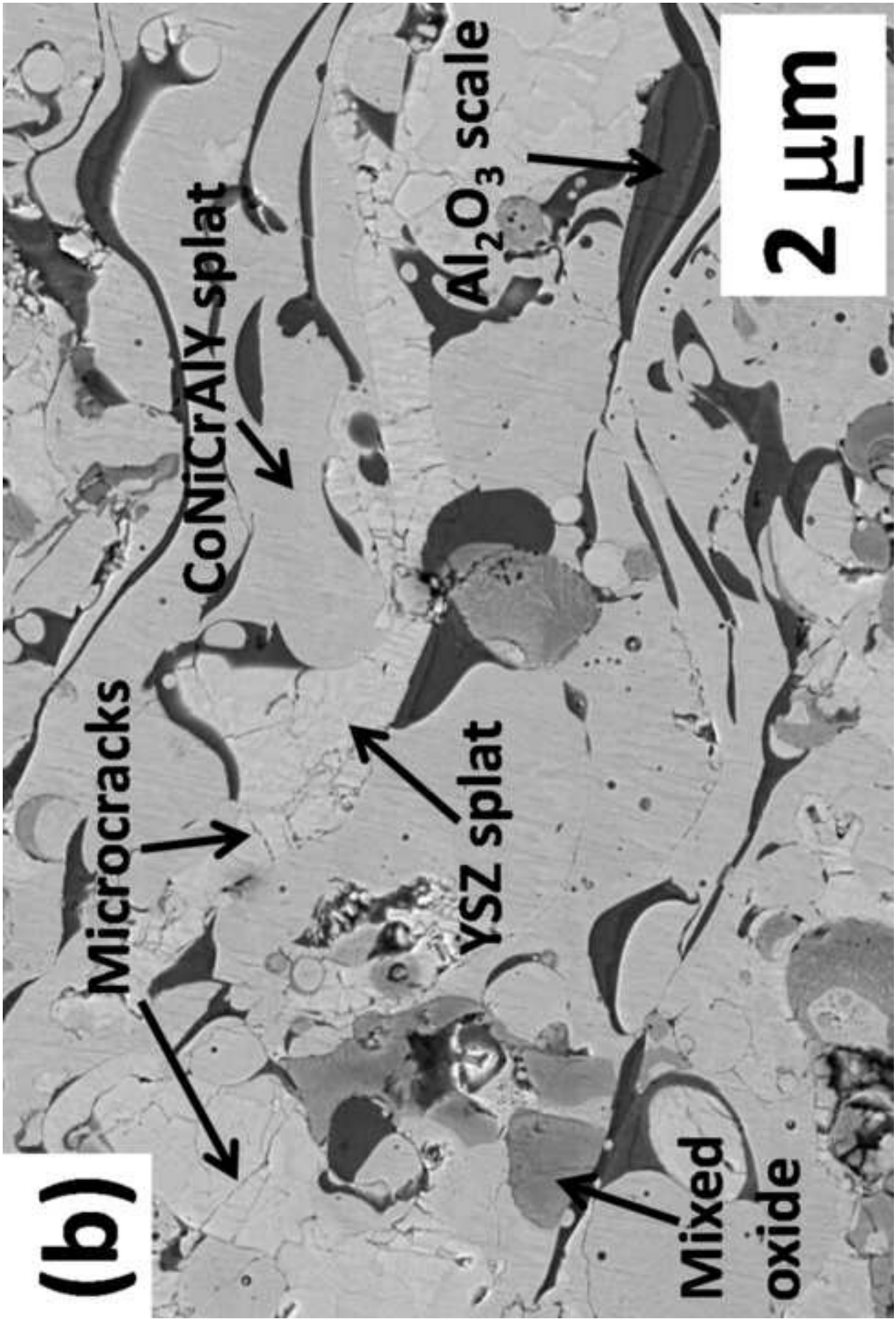
(b)
Microcracks
CoNiCrAlY splat
Al_2O_3 scale
YSZ splat
Mixed oxide
2 µm

Figure-6b

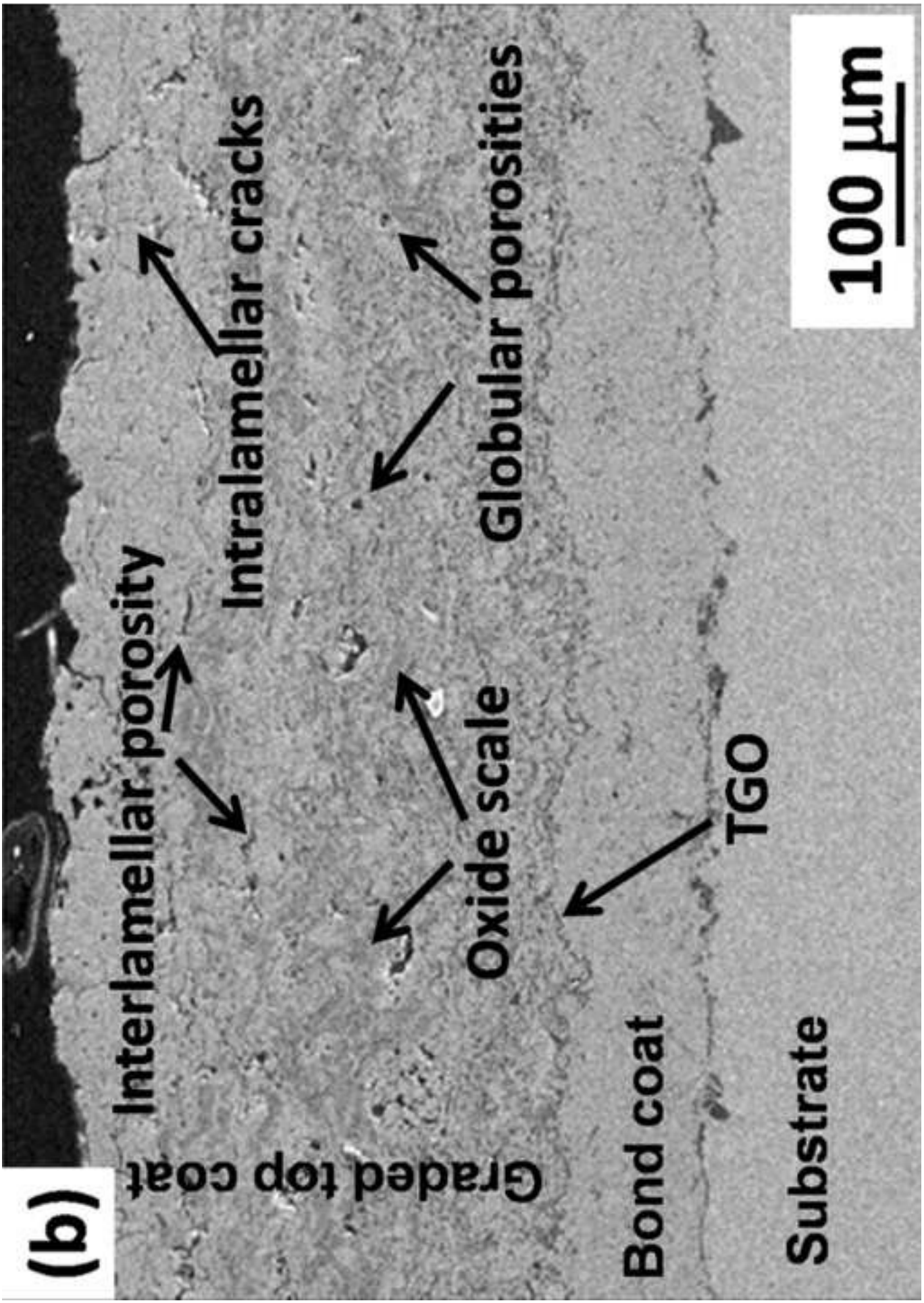
(b)
Graded top coat
Bond coat
Substrate
Interlamellar porosity
Intralamellar cracks
Oxide scale
Globular porosities
TGO
100 µm

Figure-7a

Figure-7b

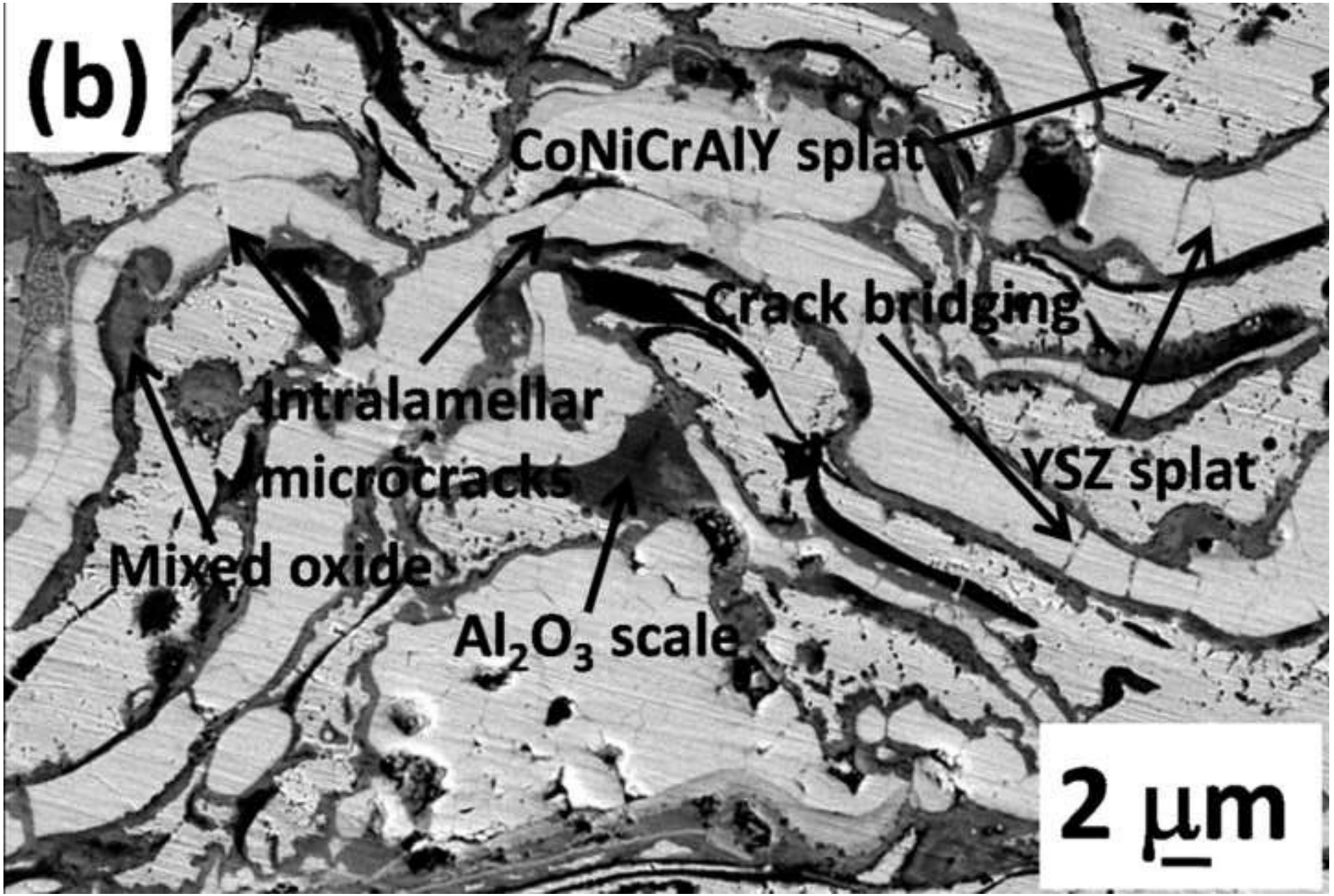

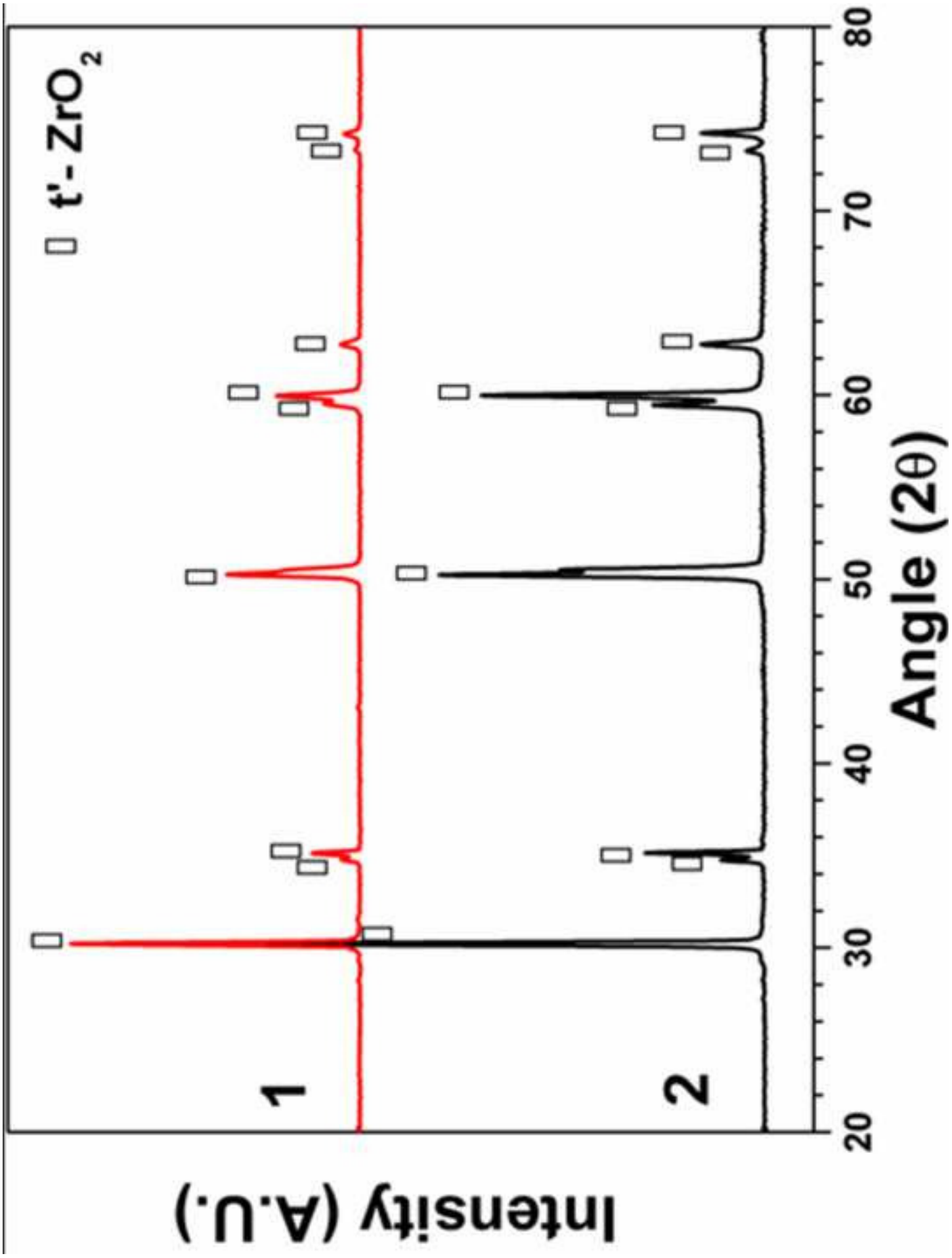

Figure-8

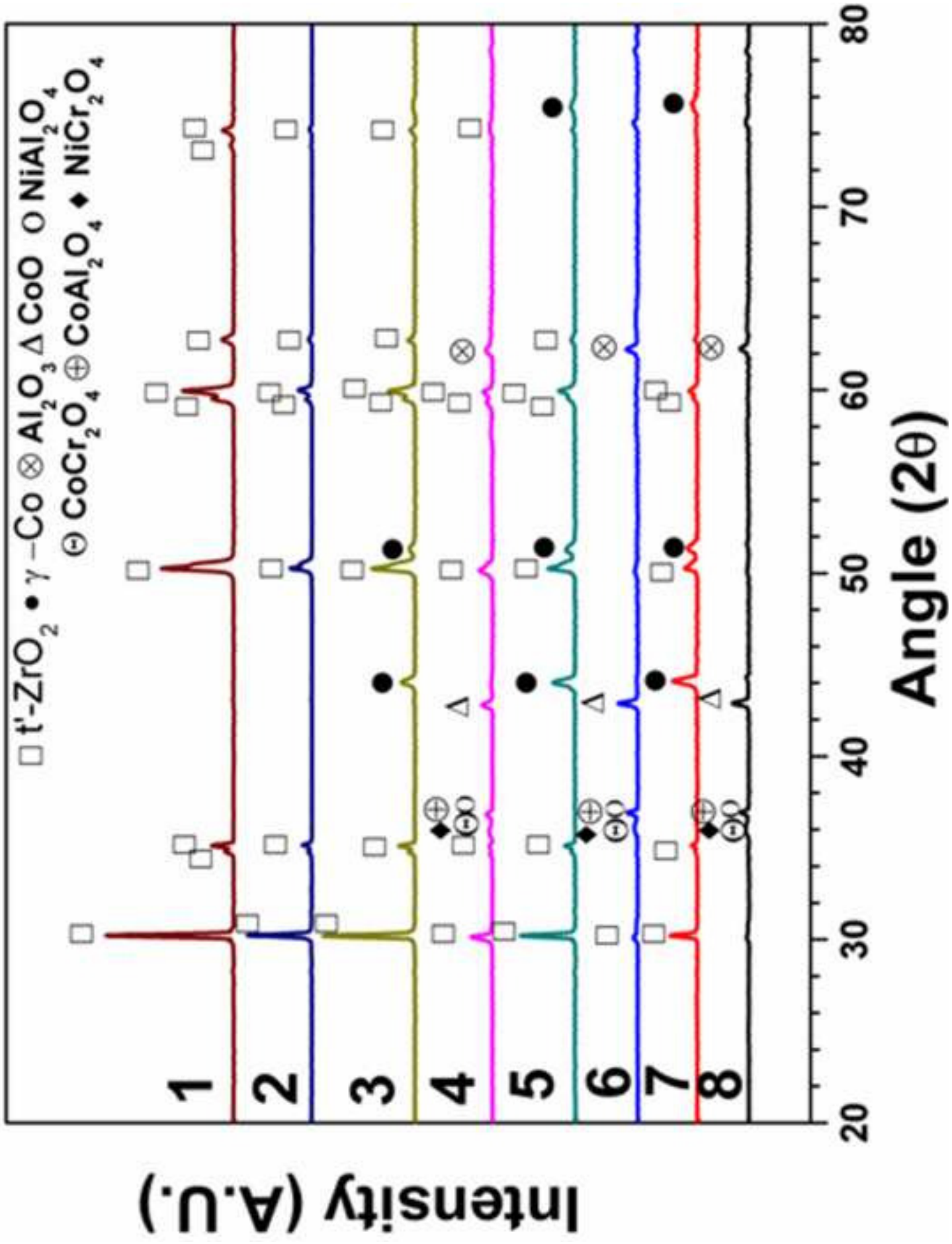
□ t'-ZrO2 • γ –Co ⊗ Al2O3 Δ CoO ○ NiAl2O4
⊖ CoCr2O4 ⊕ CoAl2O4 ◆ NiCr2O4
1
2
3
4
5
6
7
8
20
30
40
50
60
70
80
Angle (2θ)
Intensity (A.U.)

Figure-9

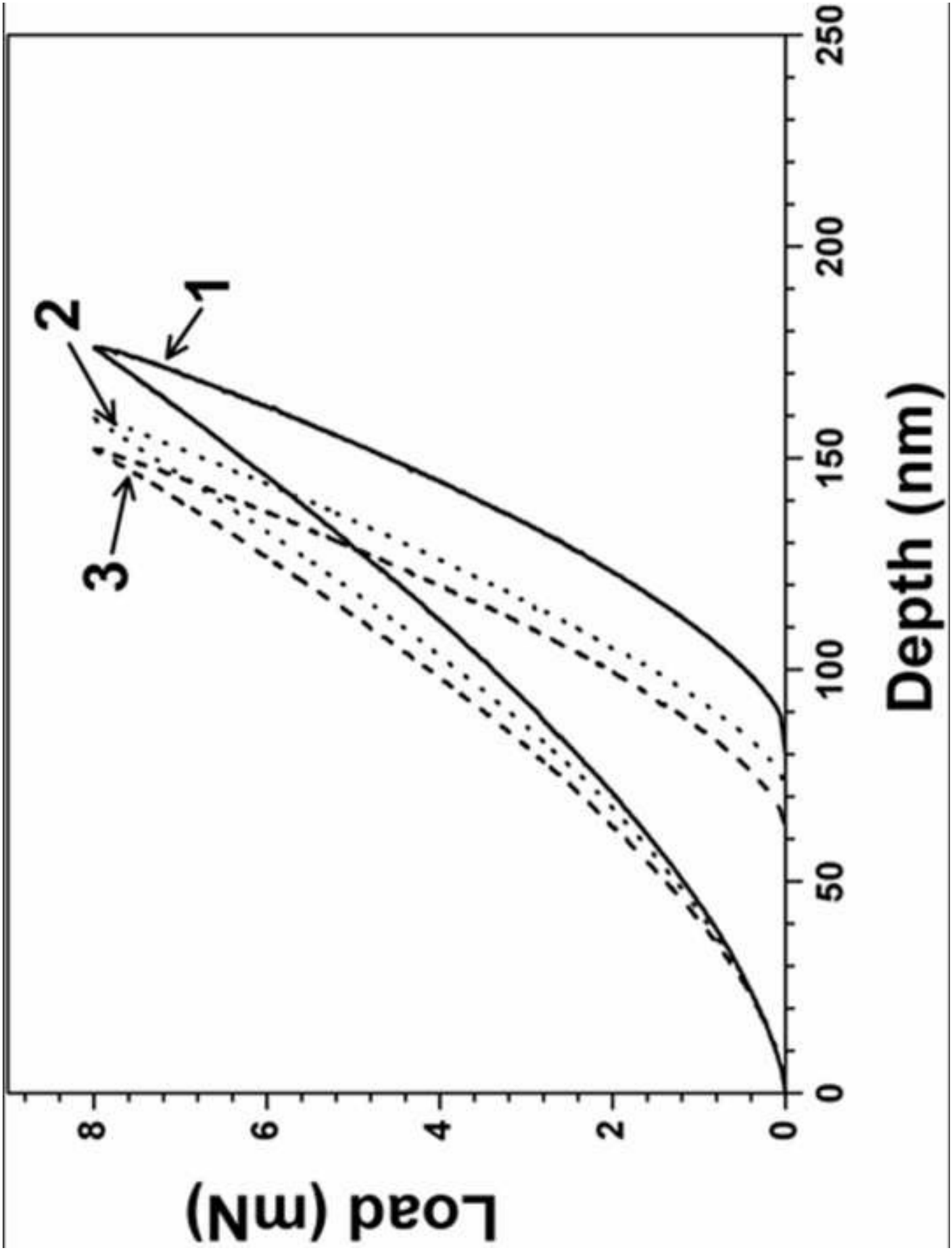

Figure-10

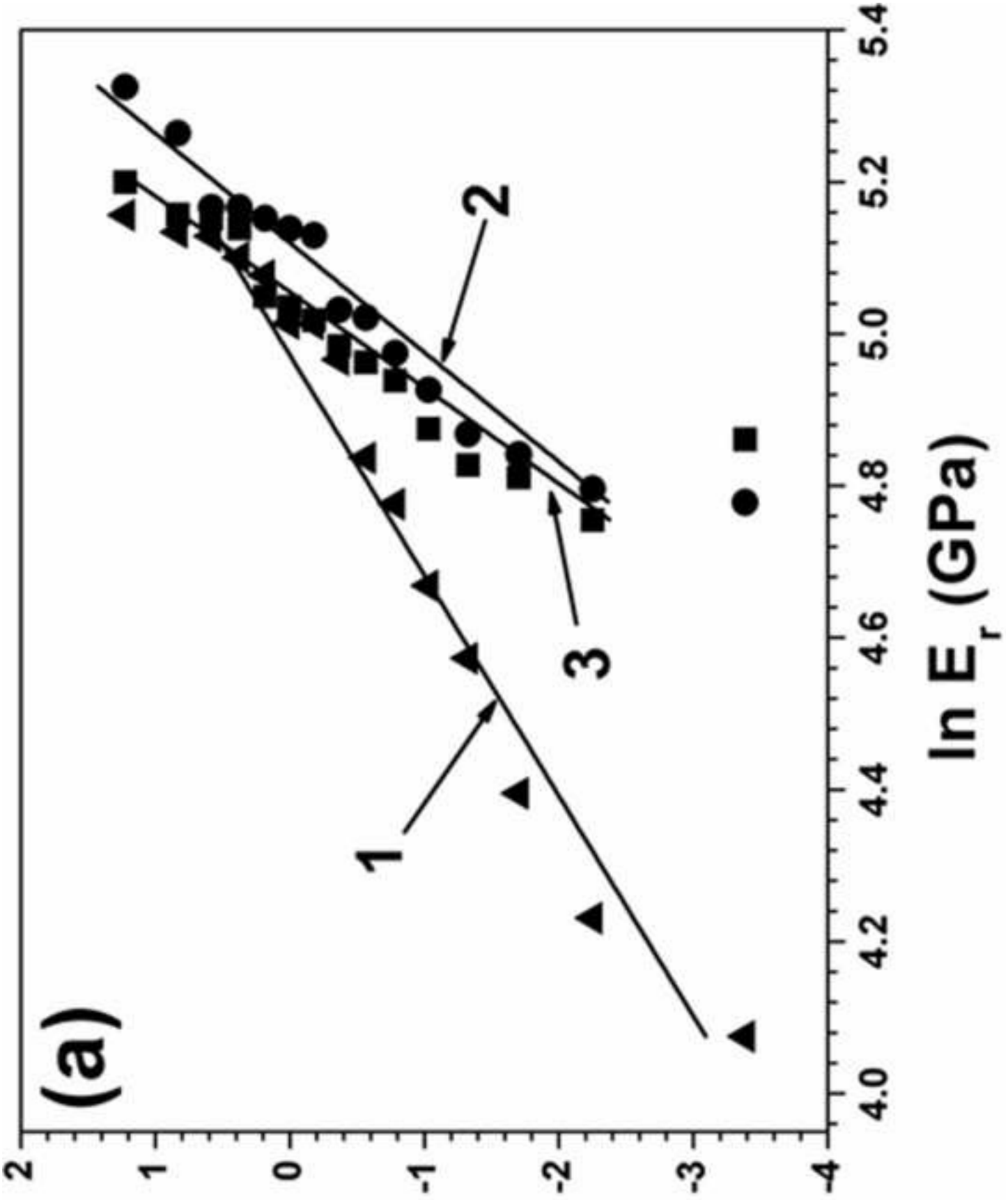

Figure-11a

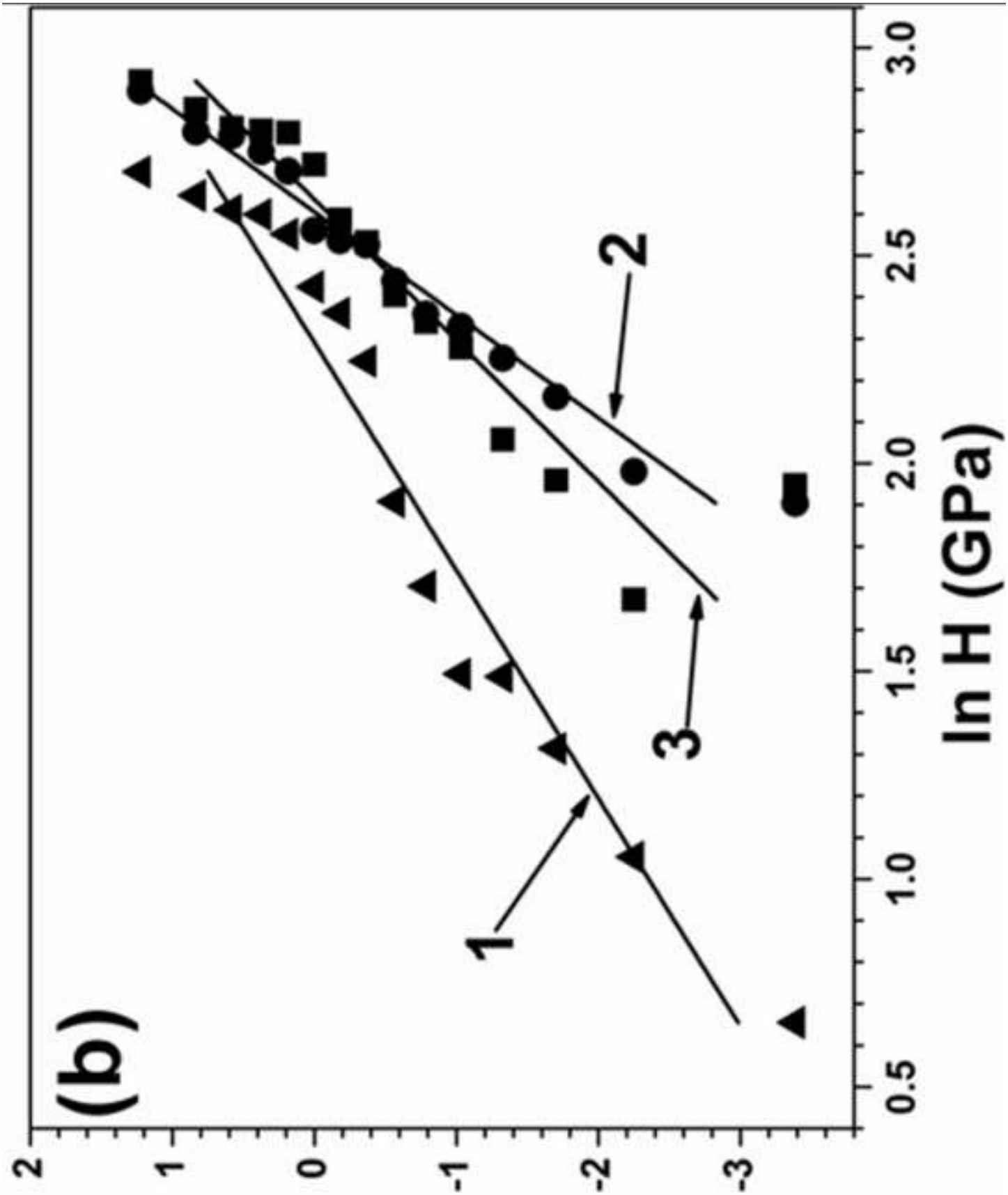

Figure-11b

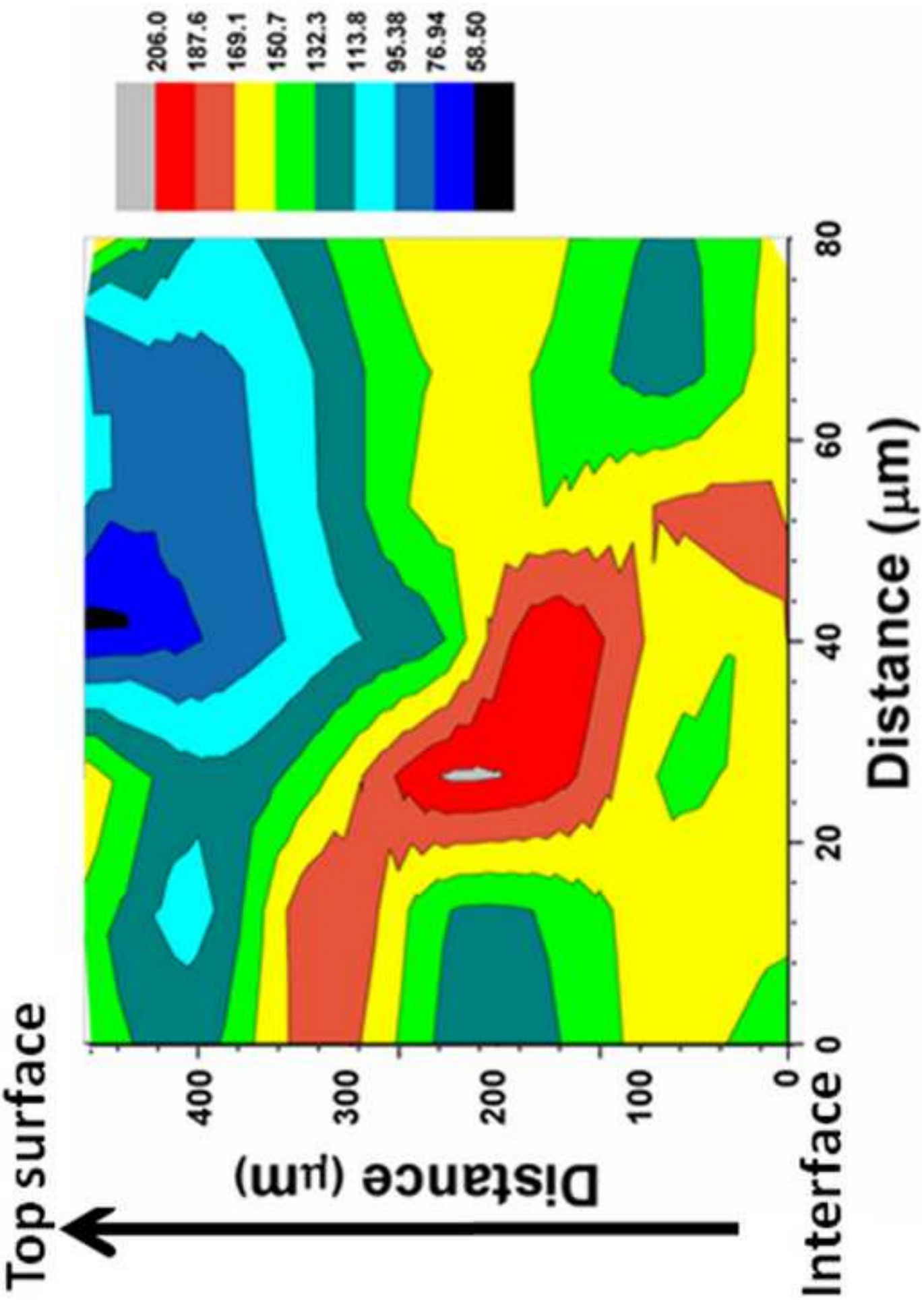

Figure-12

Figure-13

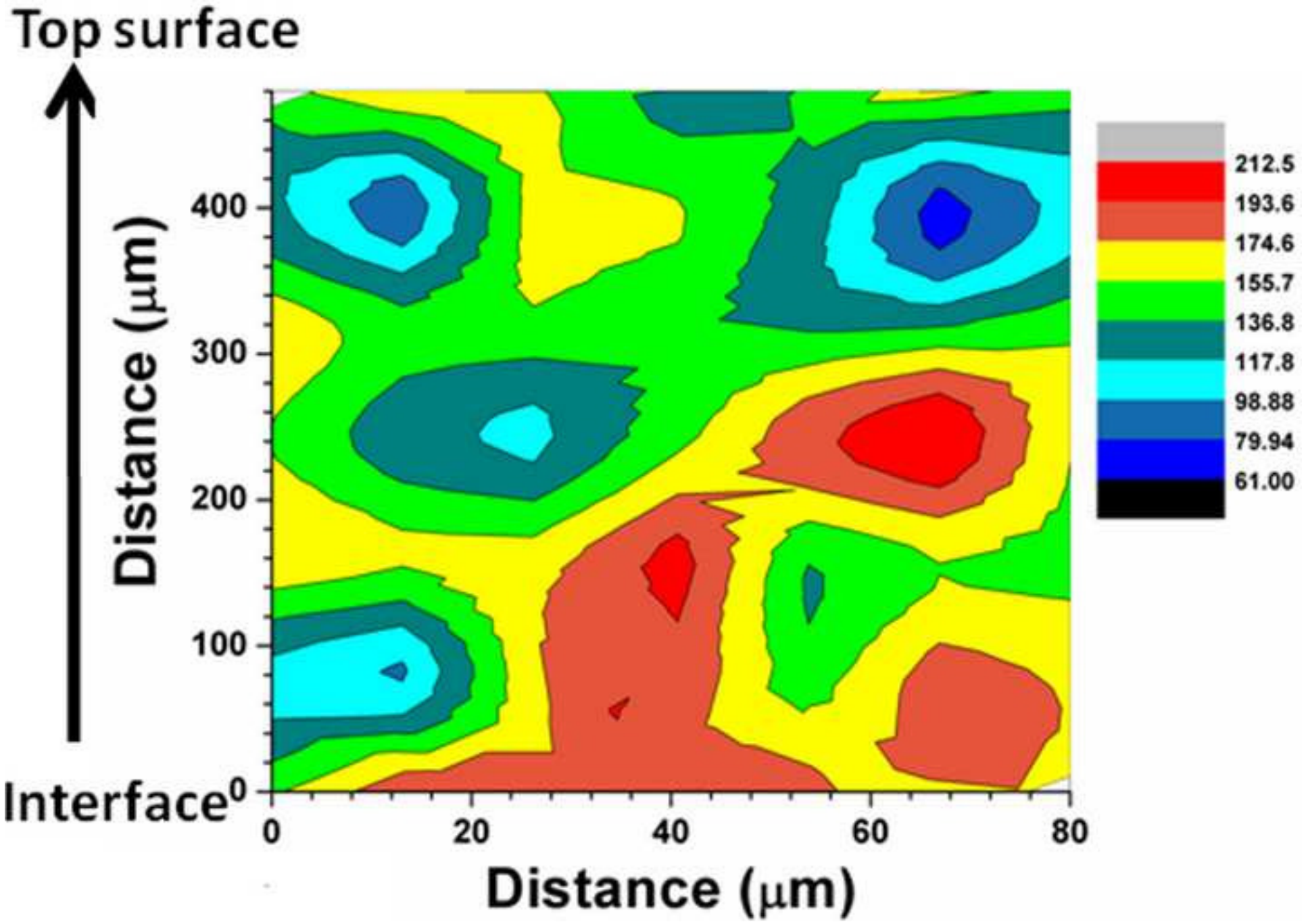

Figure-14